Research
A SCIENCE PARTNER JOURNAL

REVIEW ARTICLE

Photo-/Electrocatalytic Reduction of CO_2 Based on Ferroelectrics

Rui Wei[1†], Shun Li[2†], Andy Li[1], and Yuan-Hua Lin[1*]

[1]State Key Laboratory of New Ceramics and Fine Processing, School of Materials Science and Engineering, Tsinghua University, Beijing 100084, China. [2]School of Chemistry and Chemical Engineering, Jiangsu University, Zhenjiang 212013, China.

*Address correspondence to: linyh@tsinghua.edu.cn
†These authors contributed equally to this work.

Citation: Wei R, Li S, Li A, Lin Y-H. Photo-/Electrocatalytic Reduction of CO_2 Based on Ferroelectrics. *Research* 2025;8:Article 0843. https://doi.org/10.34133/research.0843

Submitted 27 May 2025
Revised 26 July 2025
Accepted 26 July 2025
Published 14 August 2025

Copyright © 2025 Rui Wei et al. Exclusive licensee Science and Technology Review Publishing House. No claim to original U.S. Government Works. Distributed under a Creative Commons Attribution License (CC BY 4.0).

Converting CO_2 into sustainable fuels or useful carbon-derived substances offers an effective strategy for tackling the energy crisis and combating global warming. Photo-/electrocatalytic CO_2 reduction provides a simple, energy-efficient, and environmentally friendly route compared to existing technologies. Ferroelectric materials, characterized by their unique spontaneous and switchable polarization, have emerged as promising candidate catalysts due to their controllable surface physical and chemical properties. This review commences by summarizing the mechanism underlying ferroelectric polarization-modulated photo-/electrocatalytic CO_2 reduction. We then highlight the recent key advancements in CO_2 reduction utilizing ferroelectric materials, along with their performance promotion strategies. Finally, we explore the obstacles and future perspectives in this field. This review will provide useful guidance for systematic design and advancement of effective photo-/electrocatalysts based on ferroelectric materials.

Introduction

Global climate change and the energy crisis pose challenges to the modern society. Carbon dioxide (CO_2), generated from industrial and other human activities, is the primary greenhouse gas in the atmosphere. Its emissions reached 41.6 Gt/year in 2024 (Global Carbon Budget, 2024), with its concentration directly correlated to rising global temperatures [1–4]. The escalating greenhouse effect threatens ecological sustainability and human development. Consequently, transforming CO_2 into value-added chemicals and fuels can not only effectively mitigate greenhouse gas emissions but also provide a sustainable solution for future energy demands [5,6]. In this context, developing efficient CO_2 conversion technology has emerged as a long-term solution for the circular economy and a key focus of research in materials science and chemical engineering [7–9].

In recent years, electrocatalysis and photocatalysis CO_2 reduction (CO_2RR) have demonstrated significant potential for transforming CO_2 into valuable chemicals or fuels under mild conditions [10–15]. These approaches not only contribute to the reduction of greenhouse gas but also facilitate the realization of a sustainable carbon cycle [16]. Consequently, these straterties have garnered substantial attention from researchers across a wide range of disciplines. However, great challenges hinder their practical applications. Existing electrocatalytic technologies (e.g., those using Cu-based catalysts [17]) often exhibit a Faraday efficiency of less than 30% for C_{2+} products, with overpotentials typically exceeding 450 mV. Furthermore, the process generates a substantial number of by-products, thereby posing a considerable challenge to the selective production of specific target products [18]. Additionally, it is crucial to minimize the high overpotential encountered during electrocatalysis and reduce the cost of electrocatalysts, which typically contain noble metals [19]. As for the photocatalytic process, it is confronted with multiple challenges, including a narrow range of light absorption and rapid recombination of photogenerated electron–hole pairs, which significantly impair efficiency and selectivity of CO_2RR [13,20,21].

Ferroelectric materials exhibit unique spontaneous polarization characteristics that can be reversed by an external electric field [22], making them promising for applications in sensors, capacitors, microdrivers, and other fields [23]. Recently, the potential of ferroelectric materials in improving the efficiency and selectivity of electrocatalytic and photocatalytic reactions has gained attention. Unlike conventional catalysts, which are constrained by static surfaces that hinder dynamic regulation of catalytic pathways, ferroelectric polarization-induced internal electric field in ferroelectric materials can modulate carrier transport and surface states, thereby enhancing electrocatalytic and photocatalytic performance [24]. Specifically, the internal electric field provides a strong driving force to promote electron–hole separation and migration toward opposite directions. Furthermore, the switching of spontaneous electric polarization can alter the reactivity of the catalyst's surface, allowing for tunable adsorption and binding strengths of reaction intermediates [25]. These intriguing effects make ferroelectric materials increasingly attractive in the field of photo-/electrocatalysis, especially regarding CO_2 activation and conversion [26,27].

Here, we provide a comprehensive review of the emerging field of photo-/electrochemical reduction of CO_2 using ferroelectric materials, mainly focusing on mechanistic

insights and material design strategies. We begin by outlining the fundamental principles of CO_2RR and ferroelectric materials/polarization. Next, we discuss how ferroelectric polarization enhances electrocatalytic and photocatalytic CO_2 conversion by modulating the electronic structure, surface characteristics of catalyst, and charge stransfer behavior. Subsequently, we present the state-of-the-art representative ferroelectric photo-/electrocatalysts for CO_2RR and summarize the latest advancements in performance-enhancement strategies. This review paper aims to offer an in-depth investigation of ferroelectric polarization-driven photo-/electrocatalysis, providing a new perspective on optimizing CO_2 conversion technology and advancing sustainable energy solutions.

Mechanisms of Photo-/Electrocatalytic CO_2RR Using Ferroelectrics

Ferroelectrics and ferroelectric polarization

Ferroelectrics are a category of materials characterized by spontaneous polarization, first documented by Valasek in 1921 in Rhosi salt [28]. Common ferroelectrics include perovskites (e.g., $BaTiO_3$, $BiFeO_3$, and $Na_{1-x}K_xNbO_3$) (Fig. 1A) [29–31], Bi-based layered structures [32], potassium dihydrogen phosphate (KH_2PO_4), tungsten bronze (e.g., $Ca_{0.28}Ba_{0.72}Nb_2O_6$), fluorate [e.g., polyvinylidene difluoride (PVDF)] [33], and ilmenite (e.g., $LiNbO_3$ and $LiTaO_3$) [34]. The spontaneous polarization of ferroelectrics arises from the inherent asymmetry in their crystal structure, resulting in a mismatch between positive and negative charge centers and creating an electric dipole moment [35]. When an electric field is applied, the electric dipole moments within the material are rearranged, causing the polarization direction to align with the applied electric field. This direction of polarization can be altered in response to variations in the intensity of the applied electric field.

A critical phase transition temperature exists between the polarized and nonpolarized phases of ferroelectrics, which is referred to as the Curie temperature (T_c). Below T_c, ferroelectrics exhibit spontaneous polarization and ferroelectric properties. Above T_c, ferroelectrics undergoes a phase transition into a nonpolarized phase, displaying paraelectric behavior. In contrast to conventional ferroelectrics, relaxation ferroelectrics do

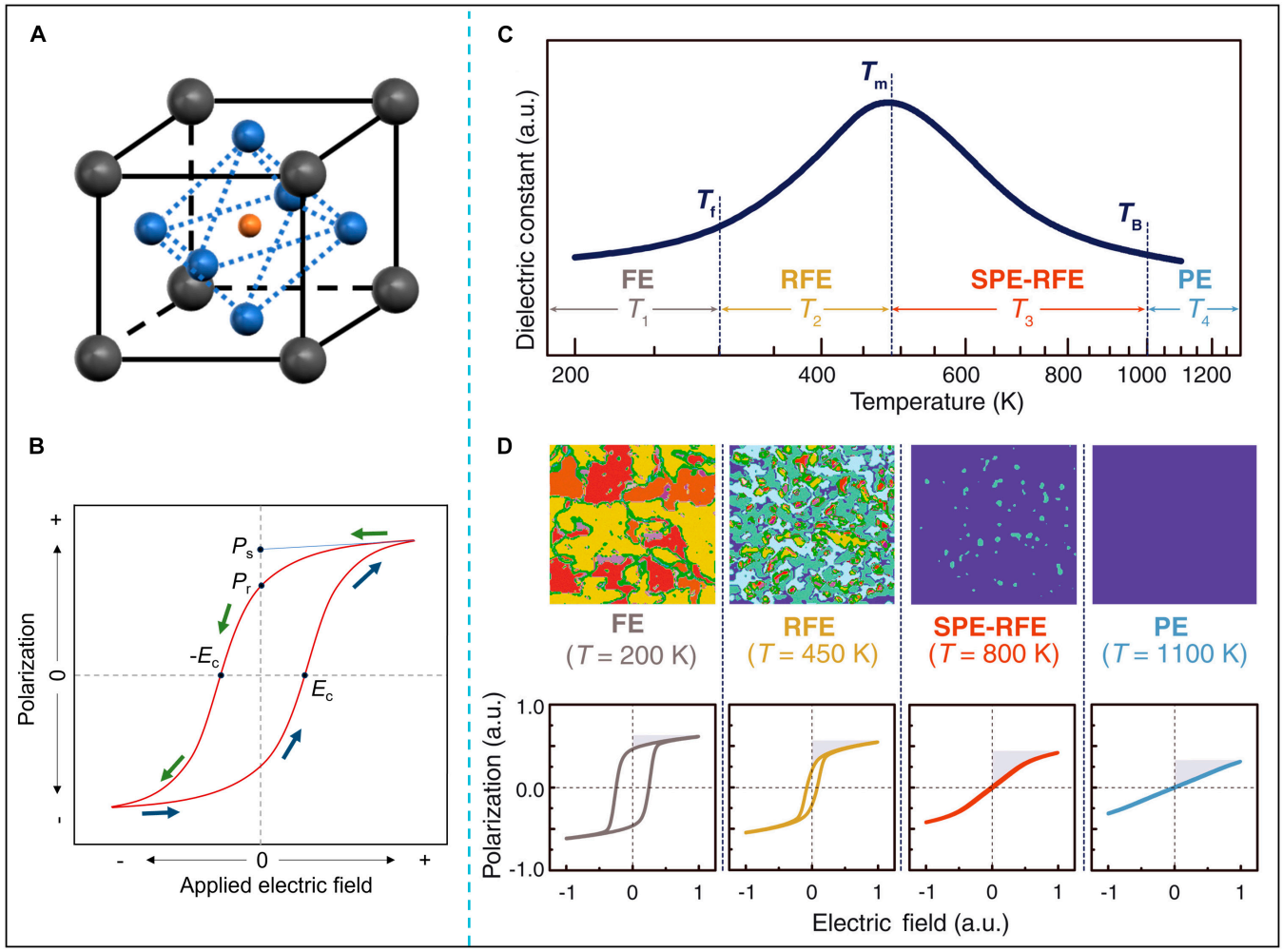


Fig. 1. Schematic illustration of (A) perovskite structure and (B) ferroelectric hysteresis loop. (C) Simulated temperature-dependent dielectric constants for Sm-doped $BiFeO_3$-$BaTiO_3$ (Sm-BFBT). T_1 to T_4 are temperature bands according to the characteristic T_f, T_m, and T_B values. (D) Simulated domain configurations and corresponding polarization–electric field (*P*–*E*) hysteresis curves demonstrate distinct characteristics of ferroelectric (FE), relaxor ferroelectric (RFE), superparaelectric RFE, and paraelectric (PE) phases. The nonpolar phase is depicted in blue, while multicolored regions correspond to domains with differing polarization orientations. Energy density distributions are represented by shaded regions within the *P*–*E* loops. Reproduced with permission from [140]. Copyright 2021 AAAS.

not possess a distinct Curie temperature. Instead, their characteristic temperature is defined as the temperature at which the maximum dielectric constant (T_m) is observed. Relaxation ferroelectrics exhibit ferroelectric phases below the freezing temperatures (T_f) and paraelectric phases above the Burns temperatures (T_B) (Fig. 1C and D). On the contrary, ferroelectric materials exhibit a characteristic nonlinear response to external electric fields, manifesting as hysteresis in the polarization–electric field (P–E) relationship (Fig. 1B). Remarkably, these materials preserve residual polarization even after field removal, demonstrating stable dipole moment retention. This unique remanent polarization property renders them particularly suitable for nonvolatile memory devices and energy-harvesting systems [36].

Mechanisms of ferroelectric polarization-modulated photo-/electrocatalytic CO_2RR

The mechanisms of photocatalytic and electrocatalytic CO_2 reduction are complex processes involving multiple steps and reaction pathways [10,37,38]. These processes aim to efficiently convert CO_2 into valuable chemicals or fuels, such as carbon monoxide (CO), methane (CH_4), formic acid (HCOOH), and methanol (CH_3OH), utilizing either light or electrical energy as the driving force. Understanding the reaction mechanism is key to modulating reaction selectivity and improving production yields.

In the photocatalytic process, as illustrated in Fig. 2A, semiconductor materials absorb photons, leading to the excitation of electrons from the valence band (VB) to the conduction band (CB), creating holes in the VB. These excited electrons then migrate to the catalyst's surface to participate in the reduction of CO_2, while the holes facilitate the oxidation of water to produce oxygen. Initially, CO_2 molecules are adsorbed onto the catalyst's surface, forming reactive intermediates such as HCOOH and CO. These intermediates can be further reduced through a variety of mechanisms, including coupled electron and proton transfer, to yield final products such as CH_3OH and CH_4 [39,40].

The electrocatalytic reaction is driven by electrical energy [41]. The mechanism can be illustrated in Fig. 2B. The reaction is typically carried out in an electrochemical cell divided into 2 parts with a Nafion film to prevent the product from being oxidized. During the electrocatalytic reaction, CO_2 is adsorbed on the surface of the electrode (commonly used electrode materials include metals such as copper, cobalt, silver, and their compounds). Electrons provided by the applied voltage are transferred to the electrode surface, where they engage in the reduction reaction of CO_2. At the same time, protons from the electrolyte are transferred to the electrode surface and combine with the electrons to form reactive intermediates. In electrocatalytic reactions, different electrode materials and reaction conditions can affect product selectivity. For example, copper-based catalysts typically produce C_{2+} products (e.g., ethanol and ethylene) [42], while silver-based catalysts primarily produce CO. Modulating the electronic structure, surface properties of the electrode materials and the reaction conditions can optimize the product selectivity and catalytic efficiency [9,43,44].

In 2004, Grosso et al. [45] first proposed the use of ferroelectrics as photocatalysts, opening up a new direction for advancing the research area of catalysis. Ferroelectric materials exhibit spontaneous polarization that generates an intrinsic electric field, which can be modulated through external thermal and electrical stimuli [46]. This built-in electric field promotes directional separation of photogenerated charge carriers (Fig. 2A), suppressing recombination losses and thereby boosting photocatalytic efficiency [24,47–49]. In the context of electrocatalysis (Fig. 2B), particularly in redox reactions involving electron gain and loss [50], the ability to absorb gases and transfer charges of the catalysts are crucial factors influencing the catalytic performance [51]. Thus, the charge-polarized surface and intrinsic electric field of ferroelectric materials critically enhance electrocatalytic performance through dual mechanisms: (i) efficient reactant activation and (ii) promoted charge carrier separation/transport, significantly boosting overall catalytic activity [52].

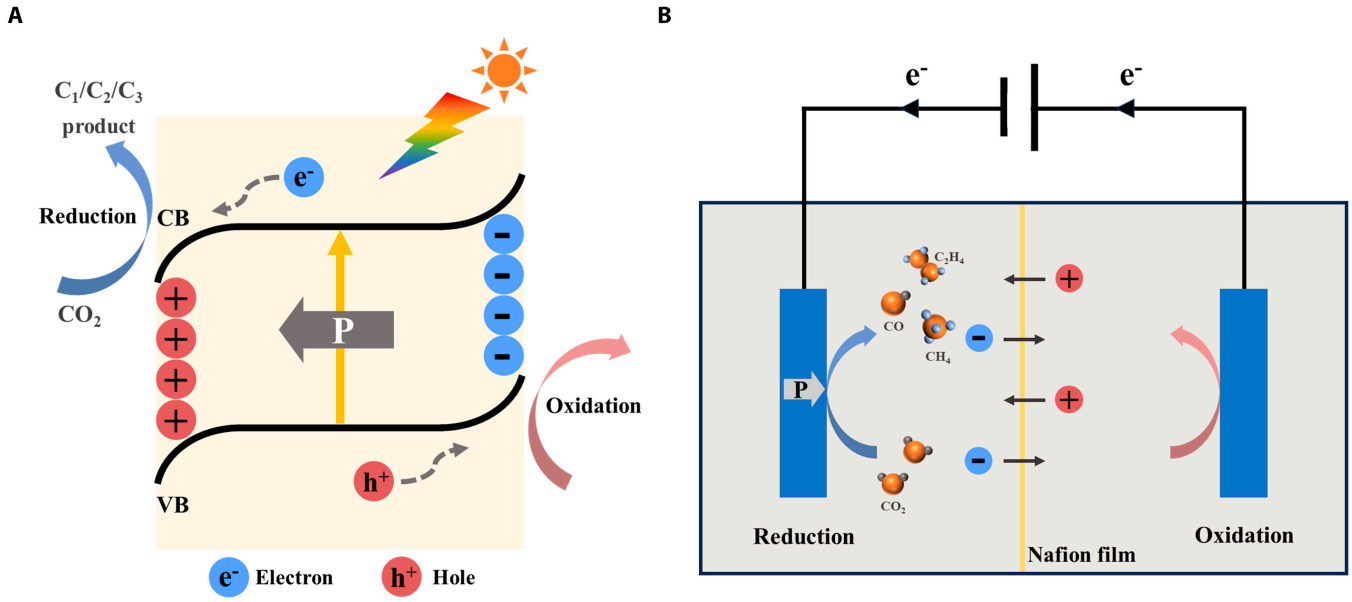


Fig. 2. Schematic illustration of ferroelectric polarization-modulated (A) photocatalytic and (B) electrocatalytic CO_2 reduction pathways.

The unique spontaneous polarization and polarization reversal characteristics of ferroelectric materials provide a novel strategy to enhance the photo-/electrocatalytic performance of CO_2RR. The tunable catalytic activity of ferroelectric catalysts mainly results from the built-in electric field and polarization effects inherent to the materials [53]. As illustrated in Fig. 3, these effects significantly affect the surface electron density/electronic structure, adsorption states of reactants and products, generation and separation of electron–hole pairs, and the transport behavior of charges, leading to changes in the catalytic reaction pathways and promoted selectivity and efficiency. The individual or synergistic effects of various factors collectively determine the product distribution and selectivity of CO_2RR. The following sections will discuss how these mechanisms influence the CO_2RR catalytic activity of ferroelectrics in detail [54].

Modulating the surface adsorption/reaction properties

Ferroelectric materials are characterized by spontaneous polarization, allowing the formation of a permanent electric dipole within the material. This creates a stable charge on the material's surface. The built-in electric field influences the distribution of surface charges, leading to an increase in adsorption capacity of reactant molecules (e.g., CO_2 and O_2) and promotion of their activation [55]. In addition, the Sabatier principle dictates that optimal catalytic efficiency depends on appropriate interactions between the catalyst's active site and the reactants [56]. Catalytic activity declines when reactant–catalyst interactions become either excessively strong or weak, highlighting the need for balanced material design. Ferroelectric systems address this challenge through polarization-state modulation, enabling precise tuning of surface chemical environments and adsorbate–catalyst interactions [57]. The polarization-switching ability of ferroelectric materials can reverse the electric field within the ferroelectric material to overcome the Sabatier limitation [58,59]. As a result, the reactant activation, surface reactivity, and reaction selectivity of the catalytic reaction can be regulated by controlling the polarization states of the ferroelectric material's surface [60], offering a novel strategy for the rational design of catalysts.

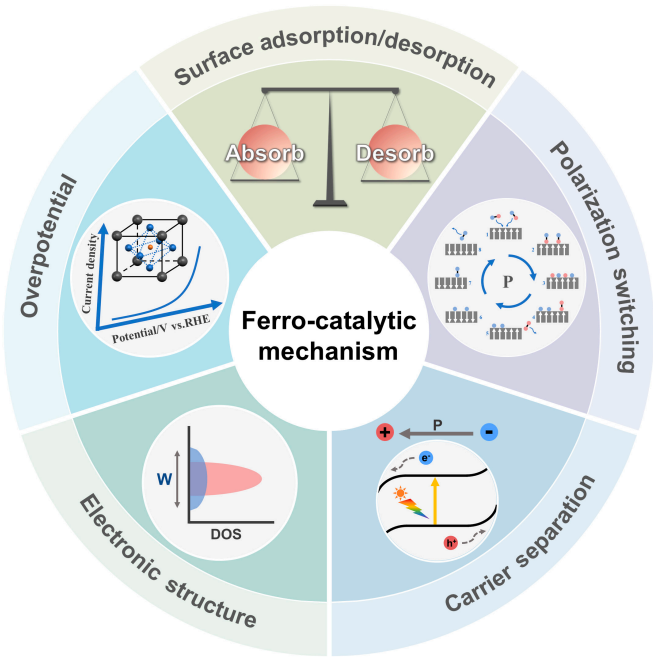


Fig. 3. Schematic diagram of ferroelectric polarization-modulated catalytic mechanisms.

Tuning the electronic structure

The electric polarization effect of ferroelectric material can significantly influence their electronic structure. The modulation of electronic states leads to the optimization of the reaction pathway and allows the catalyst to interact with the reactants in a more efficient manner, ultimately enhancing its catalytic performance. As a representative example, $BiCoO_3/Bi_5CoTi_3O_{15}$ composite catalysts illustrate how ferroelectric substrates enhance both the adsorption capacity and activation energy of the catalyst for specific molecules by providing additional electronic states [61].

In addition, it is well known that the alteration of the *d*-band center energy is closely associated with the adsorption energy of the reactants, which can significantly influence both catalytic activity and selectivity [62,63]. In ferroelectric materials, the *d*-band center may shift to different energy states as a consequence of the electric fields, which in turn influences the interaction forces and modes between the metal and the reactants [64]. As a result, the regulation of electron density on ferroelectric catalyst surfaces can effectively promote the adsorption of specific intermediates involved in catalytic reactions.

Promoting the carrier separation efficiency

Photocatalytic processes initiate through light-induced generation of electron–hole pairs in the semiconductor material [65]. Ferroelectric polarization establishes an internal electric field that induces band bending, thereby significantly suppressing charge recombination, facilitating efficient charge separation, and increasing the population of available charge carriers for surface redox reactions [66,67]. Consequently, the inherent polarization properties of ferroelectric materials can substantially enhance the efficiency of both photocatalytic and electrocatalytic CO_2 reduction processes.

Lowering the overpotential of electrocatalysis

Ferroelectric materials have been reported to effectively reduce electrocatalytic overpotentials [68], including hydrogen evolution reaction (HER) [69,70], oxygen evolution reaction (OER) [52,71], and nitrogen reduction reaction (NRR) [72]. The built-in polarization electric field significantly accelerates the adsorption and activation of reactants by intensifying the electric field at the electrode–electrolyte interface [52]. This mechanism can lower the energy barrier for electron transfer, allowing ferroelectric materials to achieve higher reaction rates at lower applied voltages, thereby enhancing the overall catalytic performance of the system. A very recent theoretical study on Mo-BN@In_2Se_3 demonstrated an electrocatalytic pathway that is contingent upon polarization flipping [73]. The limiting value of the electrocatalytic no-reducing potential on Mo-BN@P↑-In_2Se_3 is 0.09 eV, which is well below the isolated Mo-BN monolayer (0.35 V). Mo-BN@P↓-In_2Se_3 is 0.53 eV, which highlights the distinctive capacity of ferroelectric materials to lower the overpotential through reversible polarization transitions while impeding competing reactions such as HER through a built-in electric field.

Moreover, the formation of double layer reduces activation energy and facilitates electron transfer [74]. At the electrode surface, the rearrangement of ions under an electric field leads to the formation of a charge-rich double layer, thereby optimizing the interactions between the reactants and the electrode surface.

This double-layer effect is particularly significant in multi-electron conversion reactions, such as CO_2RR, as it not only optimizes the adsorption modes of the reactants but also reduces the energy consumption of the multi-step reactions [75,76].

Polarization-dependent CO_2RR pathways

The ferroelectric polarization offers precise control of the CO_2RR pathways by dynamically tuning the surface charge distribution and intermediate adsorption configuration. For instance, density functional theory (DFT) calculations reveal the critical role of polarization direction on the reaction energy: The upward polarization (P↑) in 2-dimensional (2D) ferroelectric In_2Se_3 is more favorable for driving the CO_2 activation reaction: $*CO_2 \rightarrow *OCOH$, which ultimately tends to produce methane or formic acid (Ul = 0.58 eV) [77]. In contrast, downward polarization (P↓) stabilizes the intermediate formate (*OCHO) and ultimately tends to produce methanol (Ul = 0.64 eV). This catalytic mechanism is supported by both computational and experimental investigations, making ferroelectric materials a unique class of CO_2RR catalysts with dynamically tunable reaction pathways.

Research Progress of Ferro-Catalytic Materials for CO_2RR

Ferroelectric photocatalysts

The persistent challenge of rapid charge carrier recombination in photocatalysis has motivated innovative material design strategies. Recent advances demonstrate that ferroelectric semiconductors offer a promising solution through their intrinsic polarization-induced internal electric fields, which enable anisotropic charge separation [47–49]. This section critically examines progress in photocatalytic CO_2RR over both traditional ferroelectric systems and emerging 2D materials (Table).

Traditional ferroelectric photocatalysts

Initially, investigations on ferroelectric material-based photocatalysts were mainly focused on conventional ferroelectrics, such as perovskite and Bi-based layered structures. Jia et al. [78] synthesized ferroelectric $Bi_4Ti_3O_{12}$ nanosheets via molten salt method. Photocatalytic tests revealed impressive CO_2-to-fuel conversion efficiencies, yielding CH_3OH (39.10 μmol g^{-1} h^{-1}) and CH_3CH_2OH (18.96 μmol g^{-1} h^{-1}) as primary products. The energetically favorable CB position (−1.2 V versus normal hydrogen electrode) of $Bi_4Ti_3O_{12}$ provides substantial thermodynamic impetus for CO_2RR. Photogenerated holes predominantly migrate to the $[Bi_2O_2]$ layer, while electrons primarily travel to the $[TiO_6]$ octahedral layer, facilitating the overall transformation process. In 2019, Tu et al. [79] developed a layered perovskite $SrBi_4Ti_4O_{15}$ (SBTO) nanosheets, which exhibited ferroelectric-enhanced photocatalytic CO_2 conversion performance. The maximum CH_4 production rates reached 19.8 μmol h^{-1} g^{-1} (apparent quantum yield: 1.33% at 365 nm) for SBTO nanosheets with optimized ferroelectric properties, representing superior performance relative to benchmark

Table. Comparison of CO_2RR performance of ferroelectric photocatalysts

Photocatalyst	Reaction conditions	Product	Production rate (μmol g^{-1} h^{-1})	Ferroelectric property	Reference
$Bi_4Ti_3O_{12}$ nanosheets	300 W Xe-lamp	CH_3OH	39.10	Unpolarized state	[78]
		CH_3CH_2OH	30.61		
Bi_2MoO_6 nanosheets	Solar simulator	CO	1.36	/	[92]
Polarized $Bi_4Ti_3O_{12}$ nanosheets	300 W Xe-lamp	CH_3OH	72.00	Ferroelectric polarization, $P_{max} \approx 0.6$ μC/cm^2	[78]
		CH_3CH_2OH	18.96		
$SrBi_4Ti_4O_{15}$ nanosheets	300 W Xe-lamp	CH_4	19.8	Ferroelectric polarization, $P_{max} \approx 1.3$ μC/cm^2	[79]
Polarized ultrathin-Bi_2MoO_6 nanosheets	Solar simulator	CO	14.38	Ferroelectric polarization, $P_{max} \approx 0.8$ μC/cm^2	[92]
V_S-$CuInP_2S_6$ film	Solar simulator	CH_4	82.39	Ferroelectric polarization and 2D structure	[65]
Bi_3TiNbO_9 nanosheets	300 W Xe-lamp	CO	20.91	Ferroelectric polarization and O_V engineering, $P_{max} \approx 0.15$ μC/cm^2	[102]
	300 W Xe-lamp	CH_4	0.96		
$Bi_{0.5}Na_{0.5}TiO_3$, powder	300 W Xe-lamp	CH_4	2.28	Ferroelectric polarization and O_V engineering	[103]
$BiFeO_3$-CdS sheet/particle nanocomposite	300 W Xe-lamp	CO	88	Ferroelectric polarization and heterojunction engineering	[141]
g-C_3N_4/$BaTiO_3$ nanosheet/fiber	300 W Xe-lamp	CH_3OH	18.17	Ferroelectric polarization and heterojunction engineering, $P_{max} \approx 16$ μC/cm^2	[121]
		CH_3CH_2OH	7.51		
$Bi_4Ti_3O_{12}$/Au, sheet/single-atom arrays structure	300 W Xe-lamp	CO	34.15	Ferroelectric polarization and SACs engineering, $P_{max} \approx 0.25$ μC/cm^2	[132]

photocatalysts. Complementary characterizations established a direct correlation between [100]-oriented spontaneous polarization and enhanced charge separation efficiency, accounting for the superior photocatalytic activity. Moreover, DFT calculations revealed that both electrons and holes show the smallest effective mass along the *a* axis, indicating high charge mobility facilitated by ferroelectric polarization. Additionally, Li et al. [80] reported that Bi_2MoO_6 ferroelectric nanosheets, treated by corona poling, exhibited excellent CO_2 reduction activity for CO production, achieving a rate of 14.38 μmol g^{-1} h^{-1} in a gas–solid system without the need for sacrificial agents or co-catalysts. This efficiency represents an enhancement of more than one order of magnitude compared to bulk Bi_2MoO_6. The combined approach of corona poling and layered structure significantly improves the separation of photogenerated electrons and holes while increasing the reactive sites for CO_2 adsorption, resulting in markedly enhanced photocatalytic CO_2RR activity. These findings collectively demonstrated the emerging application of ferroelectric materials for photocatalytic CO_2 conversion.

2D ferroelectric photocatalysts

Over recent decades, 2D materials have garnered significant interest in catalytic applications, particularly as electrocatalysts and photocatalysts [81–85], due to their advantageous structural and electronic characteristics. These include high surface-to-volume ratios, abundant catalytic sites, minimized charge migration distances, and adjustable electronic band structures. Among these, piezo-/ferroelectric 2D materials (e.g., SnSe, GeS, MXenes, BiOCl, $AgBiP_2Se_6$, and In_2Se_3) have been extensively studied through both experimental and computational approaches for various catalytic processes [30,54,86–90], including HER, oxygen reduction reaction (ORR), NRR, and CO_2RR. Notably, recent computational studies suggest that 2D ferroelectric heterostructures, especially those with van der Waals (vdW) interfaces, may demonstrate exceptional photocatalytic CO_2 conversion efficiency [91], which is attributed to efficient charge carrier separation and transfer enabled by robust interlayer electronic coupling.

Recent work by Chiang et al. [65] has revealed that simultaneous control of ferroelectric and spin polarizations in 2D $CuInP_2S_6$ (CIPS) can significantly enhance photocatalytic CO_2 reduction performance (Fig. 4A and B). Controlling the ferroelectric–paraelectric phase transition and applying electrical poling treatments lead to increased CO and CH_4 production with extended polarization time. Optimal product yields of 20.34 μmol g^{-1} (CO) and 39.88 μmol g^{-1} (CH_4) were achieved after 60 min of polarization during 6-h catalytic tests (Fig. 4C and D). Further performance enhancement was realized through synergistic sulfur vacancy (V_S) engineering and magnetic field application, where the spin-polarized V_S-CIPS system demonstrated substantially improved activity relative to pristine CIPS. The modified V_S-CIPS system exhibited a photocatalytic CH_4 yield of 54.9 μmol g^{-1}, which increased by 35% to 74.29 μmol g^{-1} under magnetic field (Fig. 4E and F). These findings establish a new strategy for enhancing CO_2 photoreduction in 2D ferroelectric materials through combined defect engineering and external field control. Similarly, intrinsic polarization-induced surface band edge modifications and efficient photocatalytic CO_2RR were also observed in other 2D ferroelectric systems like $CuBiP_2Se_6$ [92].

Moreover, Li and Young [93] conducted DFT calculations to study the photocatalytic CO_2RR activity of a novel 2D MXene Y_2CO_2 ferroelectric material with a suitable bandgap. The material's capability to convert CO_2 into various C_1 products, including CO, formic acid, methanol, and methane, was systematically investigated. The results revealed that on an oxygen-vacancy (O_V) defective Y_2CO_2 surface, CO_2 adsorption is strongly preferred over CO adsorption on the "poled up" surface ($E_{ads} = -2.27$ eV for CO_2 versus −2.12 eV for CO), while this preference reverses on the "poled down" surface ($E_{ads} = -1.56$ eV for CO_2 versus −2.87 eV for CO). This polarization-dependent adsorption behavior enables selective molecular adsorption control. Furthermore, the study found that methanol formation is more favorable on the "poled up" surface ($E_{ads} = -0.76$ eV for CH_3OH) compared to the "poled down" surface ($E_{ads} = -1.14$ eV), while formic acid shows stronger adsorption on the "poled down" surface ($E_{ads} = -1.40$ eV versus −0.93 eV on "poled up"). Notably, methane adsorption remains weak on both surfaces ($E_{ads} > -0.5$ eV), making CH_4 formation energetically unfavorable. This work demonstrates that 2D Y_2CO_2 MXene, with its tunable adsorption properties through polarization control, represents a highly promising and efficient catalyst for CO_2RR, providing valuable guidance for designing advanced 2D ferroelectric photocatalysts.

Engineering strategies of ferroelectric photocatalysts

For photocatalytic process, increasing the polarization field of ferroelectric catalysts can effectively modulate the surface electronic state and enhance the separation efficiency of photogenerated electron–hole pairs, offering significant potential to greatly improve the activity and selectivity of photocatalytic reactions. Consequently, the current engineering strategies for ferroelectric photocatalysts mainly focus on enhancing the polarization field, optimizing the adsorption modes and increasing surface active sites [94,95]. These strategies include engineering oxygen vacancy, constructing heterojunction, and introducing single-atom catalysts (SACs). The following section provides a comprehensive overview of the fundamental principles underlying these promotion strategies, along with the most illustrative examples reported recently.

Engineering oxygen vacancy

Oxygen vacancies (O_V) appear in oxygen-containing compounds because of the lack of oxygen atoms in the crystal lattice [96]. The O_V, acting as donor-like defects, can introduce a defect band near the CB of the metal oxide photocatalyst [97]. The presence of oxygen vacancies and the resulting saturation of metal coordination contribute to CO_2 capture and electron generation reactions, ultimately promoting the CO_2 photocatalytic reduction process [98]. The O_V in the catalyst serves as an effective adsorption site for CO_2 molecules. The insertion of an oxygen atom from the CO_2 molecule into the O_V leads to the formation of a stable adsorption complex. During the CO_2 adsorption process, the *d*-orbital of the coordinated unsaturated metal atom contributes additional electrons to the lowest unoccupied molecular orbital (LUMO) of the CO_2 molecule [99]. This electron transfer process not only increases the electron density of the CO_2 molecule but also facilitates the breaking of chemical bonds. In particular, the electron transfer induces a distortion of the CO_2

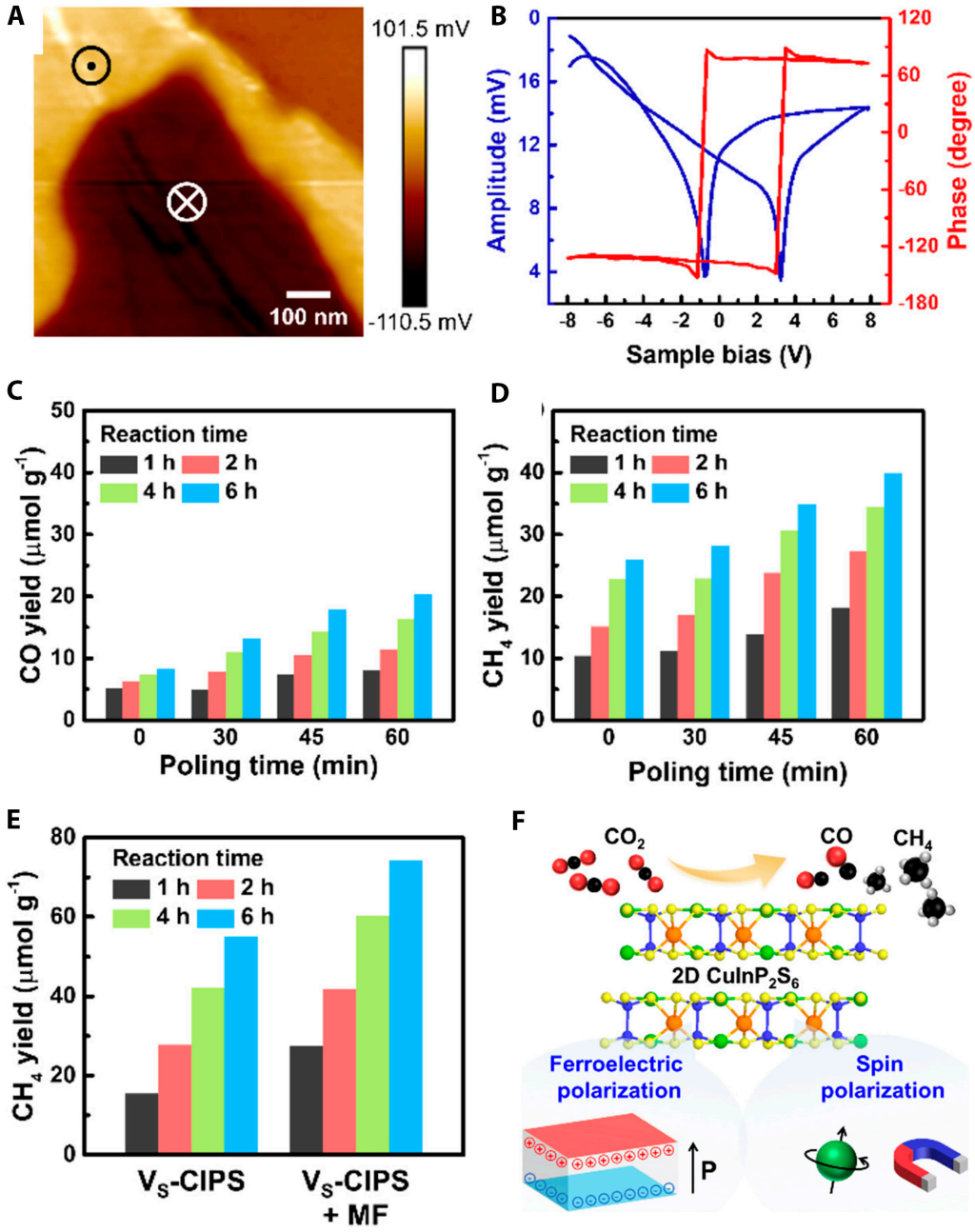


Fig. 4. Ferroelectric and spin polarization-modulated photocatalytic CO_2RR over 2D $CuInP_2S_6$ (CIPS). (A) OP-PFM [piezoresponse force microscopy (PFM) in the OP direction] characterization of a 200-nm-thick CIPS nanoflake. (B) Corresponding local hysteresis loops showing PFM amplitude and phase responses. (C) Temporal evolution of CO and (D) CH_4 generation under varying poling durations (0, 30, 45, and 60 min). (E) Comparative analysis of CH_4 yield between V_S-CIPS and magnetic field-assisted V_S-CIPS systems at different reaction time intervals (1, 2, 4, and 6 h). (F) Schematic illustration of the mechanism of ferroelectric and spin polarization promoted catalysis in 2D CIPS. Reproduced with permission from [65]. Copyright 2024, American Chemical Society.

molecule's structure, thereby reducing its chemical bonding energy and increasing its susceptibility to subsequent reaction steps [100].

Incorporating oxygen vacancies into ferroelectric materials not only enhances their ability to absorb visible light (by shifting the CB downward) but also significantly alters the materials' charge transfer characteristics [101]. As an active site, O_V plays a crucial role in modulating the photocatalytic CO_2 reduction processes. A represetative study by Zhang and colleagues [102] reported ferroelectric Bi_3NbTiO_9 (BNT) nanosheet catalysts prepared using a one-pot hydrothermal method by creating surface oxygen vacancies through corona polarization treatment. The *P*–*E* hysteresis loop reveals that corona poling treatment and O_V engineering synergistically enhance the built-in electric field polarization (Fig. 5A). Subsequent calculations reveal that the carrier density values for BNT, BNT-P, BNT-OV2, and BNT-OVP are 3.46×10^{21}, 4.44×10^{21}, 3.89×10^{21}, and 5.63×10^{21}, respectively. The flat-band potential remains unaffected by corona polarization and/or the formation of O_V. These results demonstrate that the improved charge separation efficiency of BNT-OVP stems from a synergistic combination of elevated ferroelectric spontaneous polarization and the

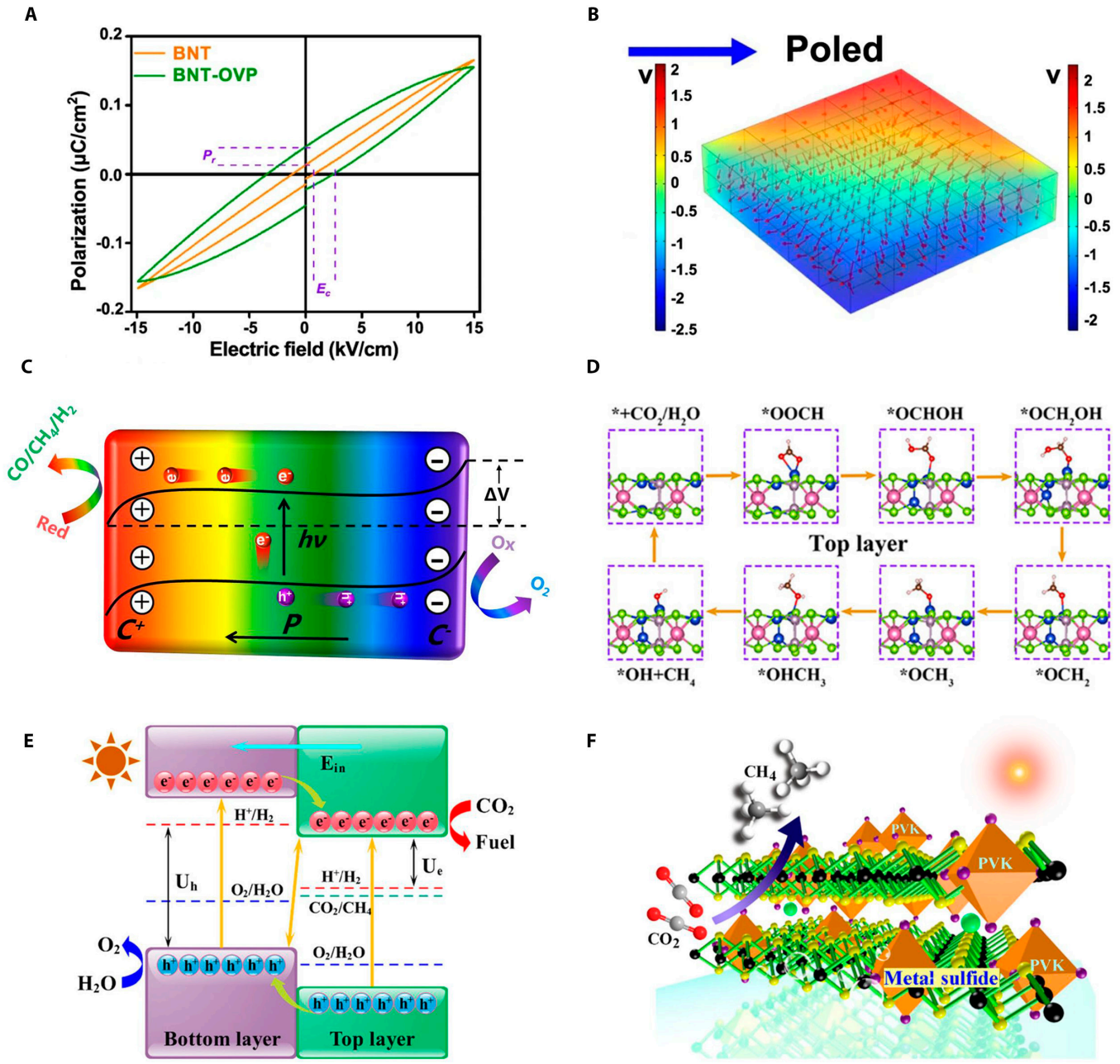


Fig. 5. (A) Ferroelectric hysteresis characteristics of pristine Bi_3NbTiO_9 (BNT) versus oxygen vacancy-engineered BNT-OVP. (B) Finite element modeling of the poling-generated internal electric field distribution in polarized BNT nanosheets. (C) Schematic illustration of the ferroelectric catalysis mechanism and tilting of energy bands under polarization field and the accompanied redox reactions. Reproduced with permission from [102]. Copyright 2021 Springer Nature. (D) Proposed reaction routes for CO_2RR. (E) Schematic diagram of the 2D ferroelectric bilayer for CO_2RR and OER. Reproduced with permission from [91]. Copyright 2021 American Chemical Society. (F) Conceptual illustration of ferroelectric–semiconductor hybrid systems employing metal sulfides for photocatalytic CO_2 conversion. Reproduced with permission from [120]. Copyright 2019 American Chemical Society.

presence of O_V. In addition, COMSOL simulations indicate that the incorporation of O_V hinders the reverse switching of domains in the BNT nanoplates, resulting in a sustained elevated residual polarization-induced electric field (Fig. 5B). The positively polarized charge facilitates the reduction reaction, while the negatively polarized charge promotes oxidation reactions (Fig. 5C). This results in an enhanced photocatalytic CO_2RR activity of the BNT nanosheets. The presence of O_V creates a "pin effect" on the switching of domain poles, which in turn affects the separation of electrons and holes. Additionally, the incorporation of O_V increases the CO_2 adsorption energy from 0.990 to 1.808 eV, supporting the idea that O_V facilitates the CO_2 adsorption and reduction process.

A very recent work by Liu et al. [103] demonstrated that introducing O_V in ferroelectric $Bi_{0.5}Na_{0.5}TiO_3$ can create a defect level, which in turn effectively modulates the band structure, reduces the barrier for carrier transport, and promotes the separation of photogenerated electron–hole pairs. Specifically, O_V engineering alters the local chemical environment of $Bi_{0.5}Na_{0.5}TiO_3$, enhancing the intensity of spontaneous

polarization through lattice distortion. Compared to other ferroelectric photocatalysts, $Bi_{0.5}Na_{0.5}TiO_3$ with O_V defects significantly enhances CO yield and product selectivity. Similarly, this strategy for constructing O_V can also be applied to other polar materials systems, such as $BiOIO_3$ nanoribbon [104], allowing it to exhibit excellent CO_2 photoreduction properties that surpass those of most reported gas–solid reaction catalytic systems.

Selective loading of co-catalyst

Anchoring co-catalysts represents a promising approach to improve the performance of photocatalytic materials [105]. Ferroelectric materials can direct the selective deposition of redox co-catalysts on different polar facet. The inherent spontaneous polarization of ferroelectric materials creates strong internal electric fields that drive the spatial separation of photogenerated charge carriers, accumulating electrons on one polar facet and holes on the opposite facet [53]. This charge separation provides a powerful driving force for the selective anchoring of reduction co-catalysts (e.g., Pt or Ag) onto the electron-rich facet and oxidation co-catalysts (TiO_2, MnO_x, or Co_3O_4) onto the hole-rich facet [106,107], thereby dramatically enhancing photocatalytic efficiency by minimizing charge recombination, providing dedicated active sites for each half-reaction, spatially separating incompatible products to prevent back-reactions, and improving overall reaction kinetics and stability.

Yang et al. [108] employed photodeposition method to load AuCu and MnO_x cocatalysts on oppositely poled facets of ferroelectric $PbTiO_3$ nanoplates. A band bending occurs along with the formation of built-in electric fields near the semiconductor–cocatalyst interfaces, together with an intrinsic ferroelectric polarization field, which provide a strong driving force for the directional drift of photogenerated electrons and holes toward AuCu and MnO_x, respectively, resulting in significantly enhanced photocatalytic activity.

Constructing ferroelectric–semiconductor heterojunctions

Heterojunctions represent interfacial regions formed by the junction of 2 dissimilar semiconductors exhibiting distinct electronic band configurations, thereby generating built-in electric fields that improve charge carrier separation and transport under illumination [109–113]. Utilizing the electric field generated in ferroelectric materials and heterojunctions to synergistically enhance the separation of electrons and holes is considered a highly promising approach for developing efficient photocatalysts [114,115]. Incorporating ferroelectric materials can regulate the degree of band bending through manipulation of spontaneous polarization and enhance the strength of the built-in electric field within the heterojunction [116].

Heterojunction photocatalysts are classified into 3 main categories: type II, type S, and type Z heterojunctions [59,117–119]. Type II heterostructures comprise 2 semiconductor materials with staggered band alignment. This energetically favorable configuration induces spontaneous spatial separation of photogenerated charge carriers, yielding enhanced photocatalytic activity beyond the capabilities of individual semiconductor components [98,115]. Implementation of this design principle in 2D CIPS bilayers demonstrated that the intrinsic polarization field effectively suppresses charge recombination with predominant CH_4 production (Fig. 5D and E) [91]. Notably, a high solar-to-fuel efficiency of 8.40% was achieved over the CIPS bilayer heterojunctions. An in situ atom-sharing strategy has been used to prepare Cs_2SnI_6/SnS_2 heterojunction. Compared to pure ferroelectric SnS_2, the photocatalytic CO_2RR performance of the heterojunction was significantly enhanced by about 5 times (Fig. 5F) [120]. This strategy can be extended to the preparation of various perovskite–metal dihalide heterostructures ($Cs_3M_2X_9/M_2Y_3$, where M = Bi, Sb; X = Br, I; Y = S, Se). Similarly, well-constructed g-$C_3N_4/BaTiO_3$ heterojunction photocatalyst also showed significantly enhanced reverse movement of photoexcited carriers due to the coupling effect of the heterojunction and ferroelectric polarization, effectively reducing the recombination and substantially improving the CO_2RR performance [121]. The classical Z-scheme configuration integrates 2 semiconductor photocatalysts with staggered band alignment coupled with an oxidation–reduction mediator system. Z-type $BiFeO_3/CsPbBr_3$ heterojunction has been demonstrated and resulted in a notable enhancement in catalytic activity [122]. Type S heterostructures are constructed by combining a reducing-type semiconductor photocatalyst with a smaller work function and higher Fermi level, and an oxidizing-type semiconductor photocatalyst with a larger work function and lower Fermi level in an offset configuration [123]. Well-designed 2D/2D S-scheme heterojunction composed of ferroelectric Bi_3TiNbO_9 and C_3N_5 nanosheets was reported, achieving efficient charge transfer through the depolarization field [124]. Further studies are needed to extend their application to CO_2

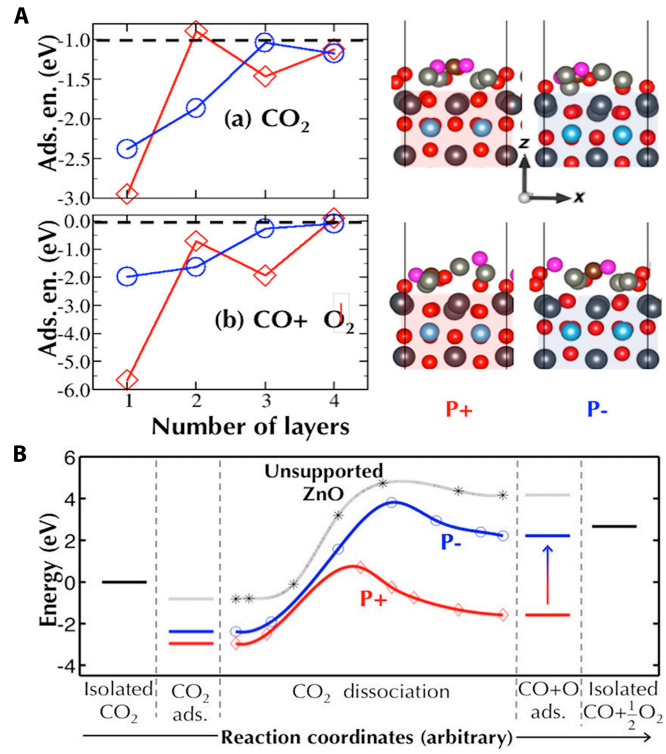


Fig. 6. (A) Dependence of CO_2 and CO + O_2 adsorption energies on $(ZnO(11\bar{2}0))_n/[2 \times 2]PbTiO_3$ as a function of layer number (n) for both positive and negative polarization states. Corresponding molecular adsorption geometries on the stoichiometric ($n = 1$) configuration are displayed on the right. (B) Comparative analysis of CO_2 dissociation pathways on pristine ZnO versus polarization-dependent $PbTiO_3$-supported ZnO catalysts. Reproduced with permission from [125]. Copyright 2016, American Chemical Society.

reduction and reveal the role of ferroelectric polarization in these composite catalysts.

Besides experimental work, theoretical simulations have also been conducted on ferroelectric–semiconductor heterostructures. For example, Alawode and Kolpak [125] introduced an innovative dynamically adjustable stoichiometric $ZnO(11\bar{2}0)_n$/$PbTiO_3$ catalytic system, where surface reactivity is modulated by the $PbTiO_3$ substrate's polarization orientation and the $ZnO(11\bar{2}0)$ layer thickness (Fig. 6). This configuration results in a substantially reduced energy pathway for CO_2 transformation. Their findings revealed pronounced variations in CO_2 adsorption energy upon polarization reversal, implying that reaction thermodynamics and reaction routes for CO_2 activation can be precisely regulated, as evidenced by the dynamic polarization-switching mechanism proposed for CO_2 dissociation on $ZnO(11\bar{2}0)/PbTiO_3$. Such a strategy may extend to more heterogeneous structures, offering new opportunities for manipulating reaction energetics.

Single-atom ferroelectric nanohybrids

The concept of SACs was first reported by Qiao et al. [126] as a novel catalyst type consisting of dispersed single metal atoms as the active centers [127,128]. The monatomic dispersion of SACs allows each isolated metal atom to participate in catalytic reactions, significantly enhancing the efficiency of chemical processes. In the CO_2RR, the highly stable molecular structure of CO_2 leads to a higher dissociation energy for the C=O bond compared to other chemical bonds, such as C–C or C–H bonds [129]. This indicates that the reduction of CO_2 requires a higher activation energy. Concurrently, the dissociation of the C=O bond requires the involvement of multiple electron and proton transfer processes, as well as complex multi-step reactions

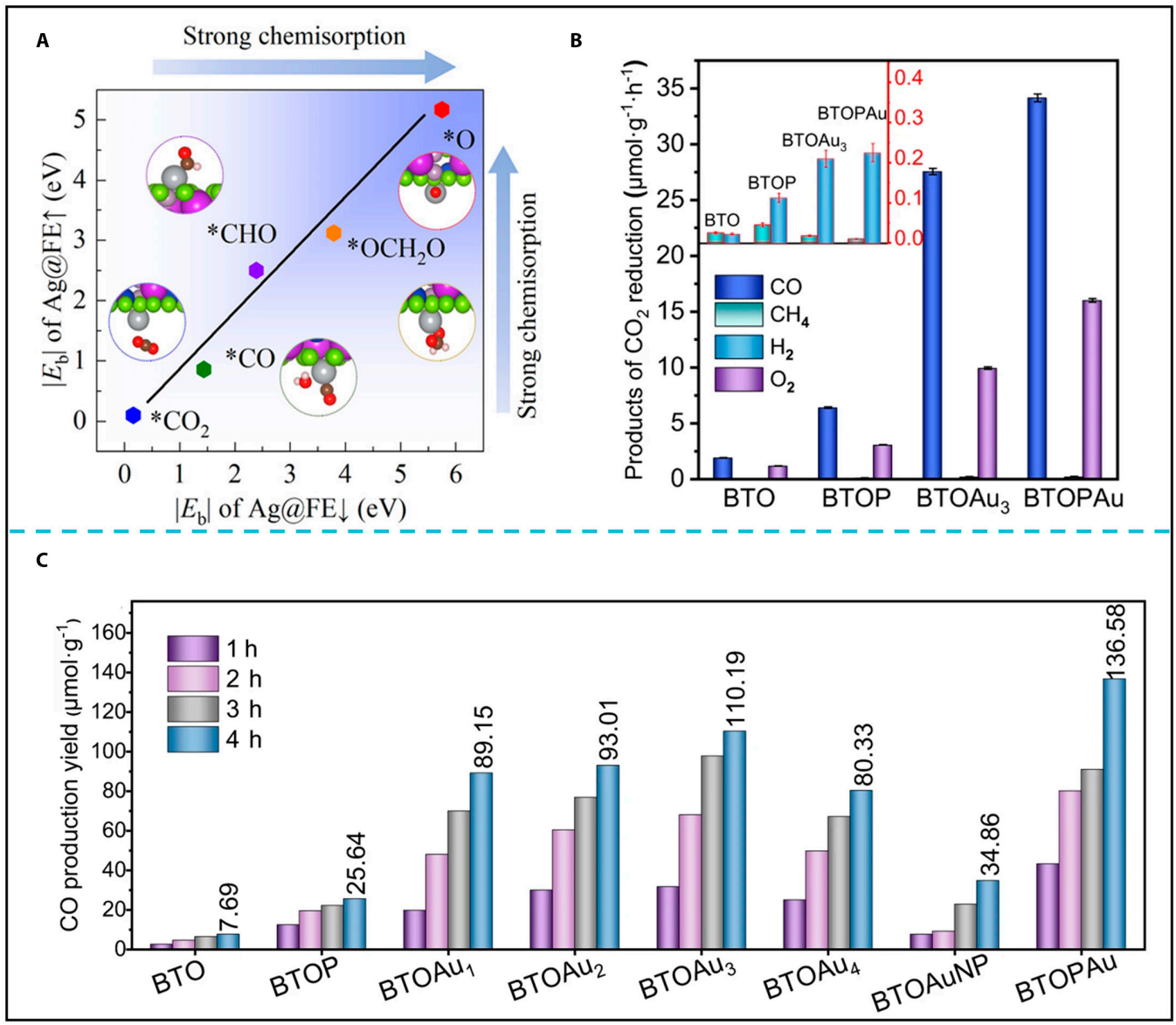


Fig. 7. (A) Conceptual illustration of polarization-modulated CO_2 reduction pathways. Reproduced with permission from [92]. Copyright 2024 American Chemical Society. (B) Evolution rates for CO, CH_4, H_2, and O_2 over BTO, poled BTOP, BTO with varying Au cluster sizes, Au nanoparticle-loaded BTO (BTOAuNP), and poled BTO with atomic Au (BTOPAu). (C) Photocatalytic CO generation efficiency in a gas–solid phase system under simulated solar light. Reproduced with permission from [132]. Copyright 2024 Springer Nature.

[130]. This makes enhancing reaction selectivity challenging. In this context, SACs utilize the unsaturated *d*-orbitals of transition metals (TMs) for electron transfer with CO_2 molecules, facilitating the formation of a more reducible intermediate and lowering the dissociation energy of the C=O bond [92]. In this sense, ferroelectric substrates provide ideal platforms for stabilizing isolated metal atoms, creating ferroelectric-supported SACs [92,131]. Such hybrid systems synergistically integrate the switchable polarization of ferroelectrics with the exceptional reactivity of atomic metal sites, leading to enhanced performance in CO_2RR with regard to both activity and product selectivity.

Jiang et al. [92] performed DFT simulations to elucidate the CO_2RR mechanism in Ag@$CuBiP_2Se_6$ system, where ferroelectric polarization cooperates with single-atom catalytic sites (Fig. 7A). Computational results reveal that the ferroelectric $CuBiP_2Se_6$ matrix generates a built-in polarization field, which drives directional charge carrier separation and transport. Meanwhile, Ag SAC anchored on the substrate can serve as an electron reservoir to modify the bonding configuration of the surface through appropriate static electron transfer, effectively promoting the adsorption and activation of CO_2 molecules. The complementary effects between the ferroelectric-induced bulk polarization and atomic-level charge regulation at Ag sites collectively enhance CO_2 capture and conversion efficiency. Notably, switching the ferroelectric polarization can selectively produce 2 different products (CH_4 or CH_3OH), providing further evidence of the feasibility of regulating the reaction pathway through a ferroelectric polarization switch.

In addition, Liu et al. [132] reported the modulation of periodic 1D Au single-atom arrays by polarization electric field of ferroelectric $Bi_4Ti_3O_{12}$ nanosheets. The Au single-atom arrays significantly reduce the Gibbs free energy for CO_2RR through Au-O=C=O-Au dual-site adsorption compared to that on Au isolated single atoms. Moreover, the Au single-atom arrays hinder the depolarization of $Bi_4Ti_3O_{12}$, maintaining a stronger driving force for separating photogenerated charges. As a result, $Bi_4Ti_3O_{12}$ with Au single-atom arrays displays a high CO production rate of 34.15 $\mu mol \cdot g^{-1} \cdot h^{-1}$, which is 18 times higher than that of pristine $Bi_4Ti_3O_{12}$ (Fig. 7B and C). More importantly, the polarization electric field proves to be a general tactic for the synthesis of 1D Pt, Ag, Fe, Co, and Ni single-atom arrays on the ferroelectric $Bi_4Ti_3O_{12}$ surface. The experimental and computational evidence collectively demonstrates that engineering ferroelectric-supported SACs establishes a dual-functional platform for optimizing both reaction kinetics and product distribution of photocatalytic CO_2 reduction.

Ferroelectric electrocatalysts

Besides intensively investigated photocatalysis, ferroelectric materials have also been applied to the field of electrocatalysis recently. In electrocatalysis, the switchable ferroelectric polarization effect can directly control gas adsorption strength, overpotential, and selectivities. In addition, it can also regulate the orbitals of the surface metal atoms. Consequently, this effect can not only activate the reactants effectively but also play a crucial role in enhancing the activity and selectivity of electrocatalytic CO_2RR [77].

The single-atom engineering strategy has also been demonstrated to be applicable to the field of electrocatalysis [133]. The switchable electric polarization in layered In_2Se_3 can dynamically tune the activation barriers, intermediate stabilization, and selectivity in electrocatalytic CO_2RR catalyzed by isolated TM atoms (Fig. 8A). Based on the single-atom ferroelectric nanohybrid construction strategy, 6 TMs, including Ni, Nb, Pd, Re, Rh, and Zr, were identified as potential catalysts for electrochemical CO_2RR using DFT calculations [77]. These findings show that the inversion of polarization in single-layer ferroelectric In_2Se_3 can regulate the energies of empty and occupied *d*-orbitals, as well as *d*-electrons of adsorbed TM atoms, thereby optimizing catalytic performance in terms of CO_2 activation, limiting potential, reaction pathway, and final

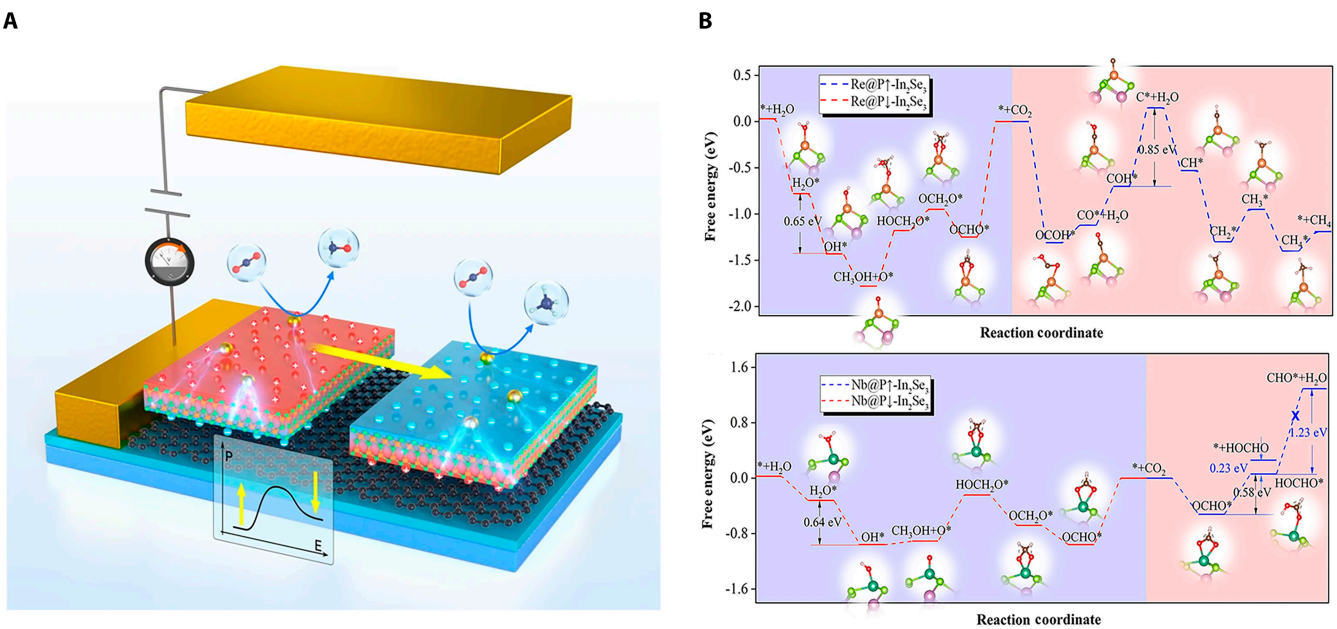


Fig. 8. (A) CO_2RR pathways on Re@In_2Se_3 and Nb@In_2Se_3. (B) Adsorption energy of the intermediate on Ag@FE↑ versus Ag@FE↓ surface. Reproduced with permission from [77]. Copyright 2021 Springer Nature.

product composition. Notably, the Re@In_2Se_3 and Nb@In_2Se_3 catalysts can selectively produce different desired products on the same catalyst through ferroelectric polarization switching (Fig. 8B). Compared to conventional nonferroelectric substrates, such as Pd@C_3N_4, TMs exhibit significantly lower limit potentials and unique ferroelectric-controllable CO_2 catalytic properties using In_2Se_3. Additionally, computational investigations employing reversible hydrogen electrode (RHE) and fixed-potential methodologies were conducted on TM single atoms (M = Fe, Co, Ni, Cu) supported on monolayer α-In_2Se_3, systematically evaluating polarization-switching effects on CO_2 electroreduction mechanisms [134]. The results indicate thermodynamic preference for *OCHO intermediate formation during CO_2 protonation, establishing this pathway as the predominant initiation step across the M@In_2Se_3 series. The computational screening identifies Co-embedded In_2Se_3 with carbon coordination (Co@In_2Se_3-C) as the optimal candidate, exhibiting the lowest theoretical overpotential (−0.385 V versus RHE) among the evaluated systems.

In addition, the synergistic effect between the metal cluster and ferroelectric substrate is anticipated to impact the CO_2RR performance substantially. Yang et al. [135] comprehensively examined CO_2 electroreduction pathways on Cu_3 trimer catalysts supported by polar Janus MoSX (X = Se, Te) monolayers using DFT calculations. The broken vertical symmetry in these Janus structures induces intrinsic out-of-plane dipoles, creating asymmetric interfacial environments for Cu_3 cluster stabilization on opposing polar facets. The computational results establish a strong correlation between substrate polarization vectors (both magnitude and orientation) and the CO_2 reduction activity of supported Cu_3 ensembles. Among all configurations, the S-terminated MoSTe-supported Cu_3 catalyst [Cu_3(S)@MoSTe] achieved peak performance for CH_4 generation, exhibiting 3.2-fold higher activity than Se-terminated counterparts. This work elucidates the pivotal influence of Janus substrate polarization on adsorbate binding energetics, where tailored interfacial electric fields optimize intermediate stabilization and overall catalytic efficiency.

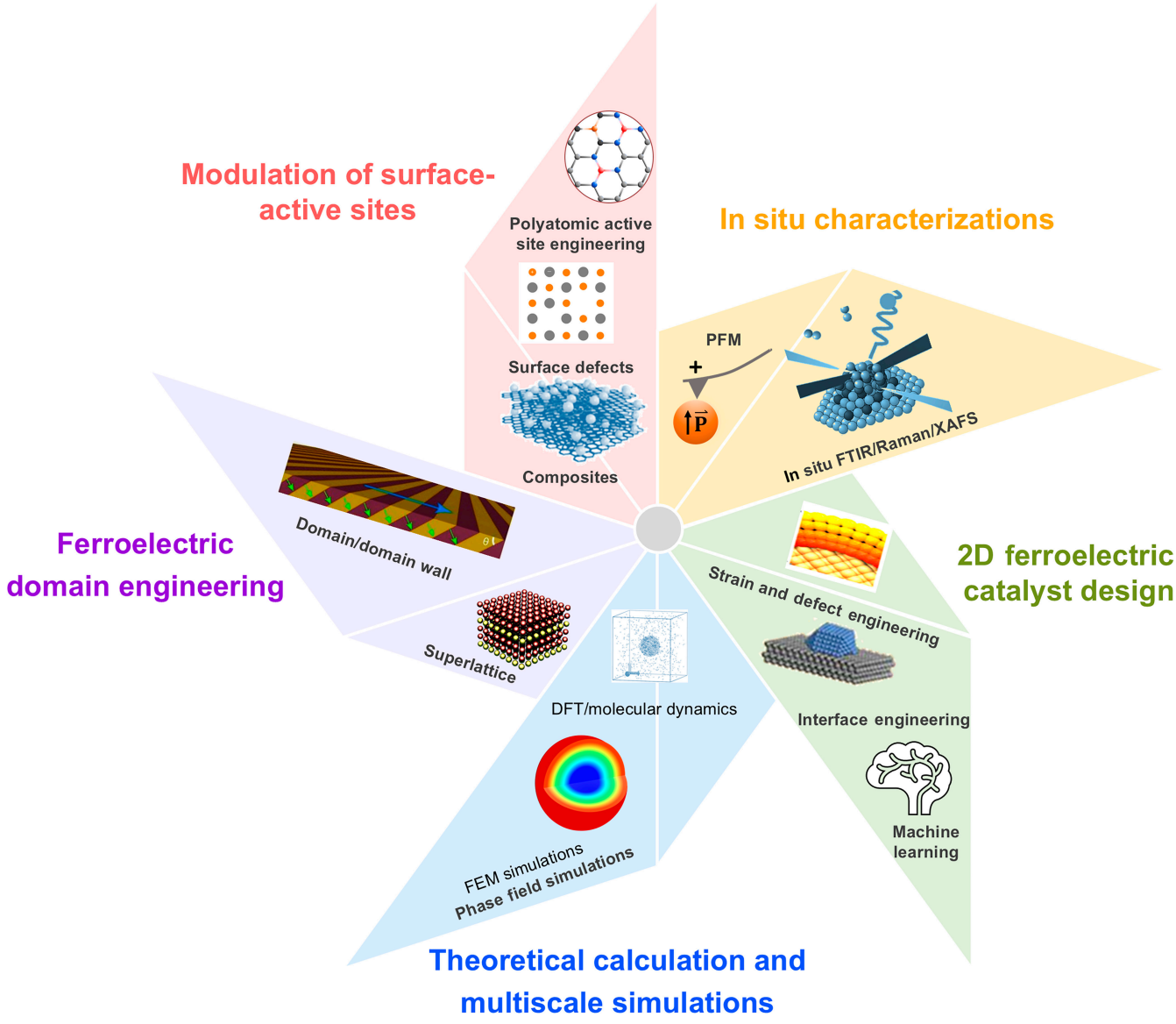


Fig. 9. Schematic illustration of future research directions in photo-/electrocatalytic CO_2RR using ferroelectric materials.

Conclusion and Perspective

Ferroelectric materials possess spontaneous polarization and reversible switching properties that enable precise modulation of catalytic activity and selectivity in CO_2 reduction for both photocatalytic and electrocatalytic pathways. These effects can significantaly tune the surface charges, electronic structure, adsorption behavior of reactants and products, and separation and migration of free charges, leading to controllable catalytic reaction pathways and enhanced photo-/electrocatalytic CO_2RR selectivity and efficiency. In this short review, we comprehensively summarized the reaction mechanisms of ferroelectric polarization-modulated CO_2RR, highlighted key advances in ferroelectrics-based photocatalyts/electrocatalysts for CO_2RR, and discussed new strategies to enhance the catalytic efficiency of ferroelectric materials. While significant progress has been made in the field of ferroelectric catalysis for CO_2RR, there are still many challenges to be addressed. Future research should focus on the design of novel high-efficient ferroelectric catalytic materials, the deeper understanding of the underlying mechanisms, and the development of synergistic strategies to achieve more efficient and selective CO_2 reduction (Fig. 9).

First, future research should prioritize the rational design and well-controlled synthesis of high-efficient ferroelectric photo/electrocatalysts. Modulation strategies of ferroelectric catalysts include creating surface defects, introducing active sites, and tuning ferroelectric domain/domain walls. In particular, the emerging 2D ferroelectrics are the most promising candidates (e.g., SnSe [136,137], GaSe, Bi_2O_2Se [138], and CIPS [65]), which can be well controlled by modulating the strain/defects to enhance the spontaneous polarization. The key industrial challenges of 2D ferroelectric catalysts include their high production costs and stability. Therefore, high-throughput screening is required to combine with machine learning algorithms to build a database of 2D ferroelectric materials (including descriptors such as band gap, polarization strength, and adsorption energy) and screen for stable and low-cost ferroelectric materials and optimal ferroelectric–co-catalyst combinations. Moreover, polarization stability degradation due to the screening effect should also be carefully addressed, which can be improved by forming a ferroelectric–semiconductor heterojunction [139].

Second, a deeper understanding of the fundamental mechanisms underlying ferroelectric photo-/electrocatalysis is essential for material design and optimization of selectivity toward desired CO_2RR products. Research should focus on identifying the key intermediates and transition states involved in these pathways and how they are influenced by the polarization field. In situ characterization techniques are desiable (e.g., electrochemical–piezoelectric force microscopy system) for directly detecting the evolution of the surface charge distribution during polarization flip in real time. Moreover, in situ spectroscopic techniques including surface-enhanced Raman spectroscopy (TR-SERS) and Fourier transform infrared (FTIR) can be used to reveal the dynamic changes of key intermediates (*COOH, *CO, etc.). Besides, multiscale simulations such as first-principles calculations and molecular dynamics simulations are required to reveal the effect of polarization direction on the energy barrier and the reaction kinetics, and finite element method (e.g., COMSOL) can be employed to simulate the electric field distributions.

Third, synergistic strategies combining multiple effects should be explored to combine ferroelectric polarization with complementary effects to improve CO_2RR performance. The optimization of ferroelectric catalysts is chiefly concerned with enhancing polarization and adsorption capacity. Vacancy engineering, heterojunctions, and SACs have been identified as effective strategies for enhancing CO_2RR activity. Consequently, further exploration is necessary to integrate diverse strategies to optimize the synergistic effect. For instance, for ferroelectric–photothermal synergy, the localized heating risks depolarization above T_c, and thus, alternative approaches (e.g., plasmonic heating below T_c, or strain-engineered thermally stable ferroelectrics) should be explored. Also, polyatomic active site engineering, which utilizes stabilizing complementary intermediates on the polarized surfaces (e.g., CO_2-activated and C–C-coupled sites), is promising for selectively form multicarbons. Moreover, spatially graded reactors need to be developed, which can tailor polarization gradients to guide reactants through optimized adsorption, activation, and desorption zones.

Acknowledgments

Funding: This work was financially supported by the Basic Science Center Project of the National Natural Science Foundation of China (grant no. 52388201) and the National Key Research and Development Program of China (grant no. 2021YFB3800601).
Competing interests: The authors declare that they have no competing interests.

References

1. Chan KS, Lo HY, Shelat VG. Carbon footprints in minimally invasive surgery: Good patient outcomes, but costly for the environment. *World J Gastrointest Surg*. 2023;15(7):1277–1285.
2. Zhang F-y, Feng Y-q, He Z-x, Xu J-w, Zhang Q, Xu K-j. Thermo-economic optimization of biomass-fired organic Rankine cycles combined heat and power system coupled CO_2 capture with a rated power of 30 kW. *Energy*. 2022;254:Article 124433.
3. Gharbi R, Gomez Vidales A, Omanovic S, Tartakovsky B. Mathematical model of a microbial electrosynthesis cell for the conversion of carbon dioxide into methane and acetate. *J CO_2 Util*. 2022;59:Article 101956.
4. Chen H, Lu J, Obobisa ES. Striving towards 2050 net zero CO_2 emissions: How critical are clean energy and financial sectors? *Heliyon*. 2023;9(12):Article e22705.
5. Bhuiyan AA, Blicblau AS, Islam AKMS, Naser J. A review on thermo-chemical characteristics of coal/biomass co-firing in industrial furnace. *J Energy Inst*. 2018;91(1):1–18.
6. Shi S, Ochedi FO, Cui S, Liu Y. Removal of CO_2 from flue gas using seaweed porous carbons prepared by urea doping and KOH activation. *Energy Fuel*. 2020;34(12):16411–16422.
7. Schuurmans JHA, Masson TM, Zondag SDA, Buskens P, Noël T. Solar-driven continuous CO_2 reduction to CO and CH_4 using heterogeneous photothermal catalysts: Recent progress and remaining challenges. *ChemSusChem*. 2023;17(4).
8. Ma Y, Wang S, Duan X. Recent advances in direct gas–solid-phase photocatalytic conversion of CO2 for porous

photocatalysts under different CO_2 atmospheres. *Chem Eng J*. 2023;455:Article 140654.
9. Chen H, Li J, Fan Q, Zheng T, Zhang Y, Yong Y-C, Fang Z. A feasible strategy for microbial electrocatalytic CO_2 reduction via whole-cell-packed and exogenous-mediator-free rGO/Shewanella biohydrogel. *Chem Eng J*. 2023;460:Article 141863.
10. Yang J, Yang K, Zhu X, Wang Z, Yang Z, Ding X, Zhong K, He M, Li H, Xu H. Band engineering of non-metal modified polymeric carbon nitride with broad spectral response for enhancing photocatalytic CO_2 reduction. *Chem Eng J*. 2023;461:Article 141841.
11. Zhang Y, Guo F, Wang K, Di J, Min B, Zhu H, Chen H, Weng Y-X, Dai J, She Y, et al. Precisely modulate interfacial Bi-O bridge bond in co-TCPP/Bi_3O_4Br to trigger long-lasting charge separation for boosting CO_2 photoreduction. *Chem Eng J*. 2023;465:Article 142663.
12. Mao D, Hu Y, Yang S, Liang J, He H, Yang S, Xu Z, Sun C, Zheng S, Jiang Z, et al. Oxygen-vacancy-induced charge localization and atomic site activation in ultrathin $Bi_4O_5Br_2$ nanotubes for boosted CO_2 photoreduction. *Chem Eng J*. 2023;452:Article 139304.
13. Ye Q, Zhou Y, Xu Y, Zhang Q, Shi X, Li D, Tian D, Jiang D. Improved charge transfer in polymeric carbon nitride synergistically induced by the aromatic rings modification and Schottky junctions for efficient photocatalytic CO_2 reduction. *Chem Eng J*. 2023;463:Article 142395.
14. Jiang H, Xu M, Zhao X, Wang H, Huo P. Fabricated local surface plasmon resonance Cu_2O/Ni-MOF hierarchical heterostructure photocatalysts for enhanced photoreduction of CO_2. *J Environ Chem Eng*. 2023;11(2):Article 109504.
15. Li C, Zhang P, Gu F, Tong L, Jiang J, Zuo Y, Dong H. Atomically dispersed Au confined by oxygen vacancies in Au-θ-Al_2O_3/Au/PCN hybrid for boosting photocatalytic CO_2 reduction driven by multiple built-in electric fields. *Chem Eng J*. 2023;476:Article 146514.
16. Peter SC. Reduction of CO_2 to chemicals and fuels: A solution to global warming and energy crisis. *ACS Energy Lett*. 2018;3(7):1557–1561.
17. Wu H, Huang L, Timoshenko J, Qi K, Wang W, Liu J, Zhang Y, Yang S, Petit E, Flaud V, et al. Selective and energy-efficient electrosynthesis of ethylene from CO_2 by tuning the valence of Cu catalysts through aryl diazonium functionalization. *Nat Energy*. 2024;9(4):422–433.
18. Sikdar N. Electrochemical CO_2 reduction reaction: Comprehensive strategic approaches to catalyst design for selective liquid products formation. *Chemistry*. 2024;30(66):Article e202402477.
19. Liang S, Huang L, Gao Y, Wang Q, Liu B. Electrochemical reduction of CO_2 to CO over transition metal/N-doped carbon catalysts: The active sites and reaction mechanism. *Adv Sci*. 2021;8(24):Article 2102886.
20. Chen X, Peng X, Jiang L, Yuan X, Yu H, Wang H, Zhang J, Xia Q. Recent advances in titanium metal–organic frameworks and their derived materials: Features, fabrication, and photocatalytic applications. *Chem Eng J*. 2020;395: Article 125080.
21. Wang H, Jiang H, Wang H, Liu Q, Huo P. NiS cocatalyst–modified ZnIn2S4 as ohmic-junction photocatalyst for efficient conversion of CO_2. *Energ Technol*. 2022;10(6):2101158.
22. Wang W, Meng Y, Wang W, Zhang Y, Li B, Yan Y, Gao B, Ho JC. 2D ferroelectric materials: Emerging paradigms for next-generation ferroelectronics. *Mater Today Electron*. 2023;6:Article 100080.
23. Martin LW, Rappe AM. Thin-film ferroelectric materials and their applications. *Nat Rev Mater*. 2016;2(2):Article 16087.
24. Guo Y, Shi W, Zhu Y. Internal electric field engineering for steering photogenerated charge separation and enhancing photoactivity. *EcoMat*. 2019;1(1):Article e12007.
25. Wang L, Huang X, Han M, Lyu L, Li T, Gao Y, Zeng Q, Hu C. Efficient inhibition of photogenerated electron-hole recombination through persulfate activation and dual-pathway degradation of micropollutants over iron molybdate. *Appl Catal B Environ*. 2019;257:Article 117904.
26. Ju L, Tang X, Kou L. Polarization boosted catalysis: Progress and outlook. *Microstructures*. 2022;2:Article 2022008.
27. Ding W, Lu J, Tang X, Kou L, Liu L. Ferroelectric materials and their applications in activation of small molecules. *ACS Omega*. 2023;8(7):6164–6174.
28. Valasek J. Piezo-electric and allied phenomena in Rochelle salt. *Phys Rev*. 1921;17(4):475.
29. Li Z, Xun W, Huang X, Wan Y, Liu Y, Gu S, He W, Yang W, Lin Z, Wang B, et al. Significant enhancement of ferroelectric performance in lead-free $NaNbO_3$ ceramics. *Ceram Int*. 2024;50(19):36487–36494.
30. Wan TL, Liu J, Tan X, Liao T, Gu Y, Du A, Smith S, Kou L. Rational design of 2D ferroelectric heterogeneous catalysts for controllable hydrogen evolution reaction. *J Mater Chem A*. 2022;10(41):22228–22235.
31. Li W, Fang B, Zhang S, Lu X, Ding J. Electrical performance and conduction mechanism of potassium sodium Niobate-based lead-free piezoceramics via two-step sintering route. *Integr Ferroelectr*. 2022;230(1):8–22.
32. Yang Q, Hu J, Fang Y-W, Jia Y, Yang R, Deng S, Lu Y, Dieguez O, Fan L, Zheng D, et al. Ferroelectricity in layered bismuth oxide down to 1 nanometer. *Science*. 2023;379(6638):1218–1224.
33. Zhang Y, Bowen CR, Deville S. Ice-templated poly(vinylidene fluoride) ferroelectrets. *Soft Matter*. 2019;15(5):825–832.
34. Vilarinho PM, Barroca N, Zlotnik S, Félix P, Fernandes MH. Are lithium niobate ($LiNbO_3$) and lithium tantalate ($LiTaO_3$) ferroelectrics bioactive? *Mater Sci Eng C*. 2014;39:395–402.
35. Wu J, Wu T. A bright new world of ferroelectrics: Magic of spontaneous polarization. *ACS Appl Mater Interfaces*. 2020;12(47):52231–52233.
36. Zhou Z, Wei R, Zhou X, Liu Y, Zhang D, Lin Y-H. Chemical bonding engineering: insights into physicochemical performance optimization for energy-storage/conversion. *Acc Mater Res*. 2024;5(12):1571–1582.
37. Tian J, Zhong K, Zhu X, Yang J, Mo Z, Liu J, Dai J, She Y, Song Y, Li H, et al. Highly exposed active sites of Au nanoclusters for photocatalytic CO_2 reduction. *Chem Eng J*. 2023;451:Article 138392.
38. Zhang S, Fan Q, Xia R, Meyer TJ. CO_2 reduction: From homogeneous to heterogeneous electrocatalysis. *Acc Chem Res*. 2020;53(1):255–264.
39. Azaiza-Dabbah D, Vogt C, Wang F, Masip-Sánchez A, de Graaf C, Poblet JM, Haviv E, Neumann R. Molecular transition metal oxide electrocatalysts for the reversible carbon dioxide-carbon monoxide transformation. *Angew Chem Int Ed Engl*. 2022;61(5):Article e202112915.

40. Xu Y, Li S, Chen M, Zhang J, Rosei F. Carbon-based nanostructures for emerging photocatalysis: CO_2 reduction, N_2 fixation, and organic conversion. *Trends Chem*. 2022;4(11):984–1004.
41. Du C, Wang X, Chen W, Feng S, Wen J, Wu YA. CO_2 transformation to multicarbon products by photocatalysis and electrocatalysis. *Mater Today Adv*. 2020;6:Article 100071.
42. Wang Z, She X, Yu Q, Zhu X, Li H, Xu H. Minireview on the commonly applied copper-based electrocatalysts for electrochemical CO_2 reduction. *Energy Fuel*. 2021;35(10):8585–8601.
43. Han GH, Bang J, Park G, Choe S, Jang YJ, Jang HW, Kim SY, Ahn SH. Recent advances in electrochemical, photochemical, and photoelectrochemical reduction of CO_2 to C_{2+} products. *Small*. 2023;19(16):Article 2205765.
44. She X, Zhai L, Wang Y, Xiong P, Li MM-J, Wu T-S, Wong MC, Guo X, Xu Z, Li H, et al. Pure-water-fed, electrocatalytic CO_2 reduction to ethylene beyond 1,000 h stability at 10 A. *Nat Energy*. 2024;9(1):81–91.
45. Grosso D, Boissière C, Smarsly B, Brezesinski T, Pinna N, Albouy PA, Amenitsch H, Antonietti M, Sanchez C. Periodically ordered nanoscale islands and mesoporous films composed of nanocrystalline multimetallic oxides. *Nat Mater*. 2004;3(11):787–792.
46. Lv T, Li J, Arif N, Qi L, Lu J, Ye Z, Zeng Y-J. Polarization and external-field enhanced photocatalysis. *Matter*. 2022;5(9):2685–2721.
47. Li S, Zhao Z, Zhao J, Zhang Z, Li X, Zhang J. Recent advances of ferro-, piezo-, and pyroelectric nanomaterials for catalytic applications. *ACS Appl Nano Mater*. 2020;3(2):1063–1079.
48. Yu D, Liu Z, Zhang J, Li S, Zhao Z, Zhu L, Liu W, Lin Y, Liu H, Zhang Z. Enhanced catalytic performance by multi-field coupling in $KNbO_3$ nanostructures: Piezo-photocatalytic and ferro-photoelectrochemical effects. *Nano Energy*. 2019;58:695–705.
49. Li S, Zhang J, Zhang B-P, Huang W, Harnagea C, Nechache R, Zhu L, Zhang S, Lin Y-H, Ni L, et al. Manipulation of charge transfer in vertically aligned epitaxial ferroelectric $KNbO_3$ nanowire array photoelectrodes. *Nano Energy*. 2017;35:92–100.
50. Francke R, Little RD. Redox catalysis in organic electrosynthesis: Basic principles and recent developments. *Chem Soc Rev*. 2014;43(8):2492–2521.
51. Mahajan C, Hasannaeimi V, Neuber N, Wang X, Busch R, Gallino I, Mukherjee S. Model metallic glasses for superior electrocatalytic performance in a hydrogen oxidation reaction. *ACS Appl Mater Interfaces*. 2023;15(5):6697–6707.
52. Wu J, Gao X, Chen Z. Elucidating the construction and modulation of built-in electric field in the oxygen evolution reaction. *Chem Eng J*. 2024;492:Article 152241.
53. Wan TL, Ge L, Pan Y, Yuan Q, Liu L, Sarina S, Kou L. Catalysis based on ferroelectrics: Controllable chemical reaction with boosted efficiency. *Nanoscale*. 2021;13(15):7096–7107.
54. Ju L, Shang J, Tang X, Kou L. Tunable photocatalytic water splitting by the ferroelectric switch in a 2D $AgBiP_2Se_6$ monolayer. *J Am Chem Soc*. 2019;142(3):1492–1500.
55. Ni C, Wang K, Jin L, Liu Y, Chen J, Yang L, Ji C, Xu H, Li Z, Tian L. Built-in electric field guides oxygen evolution electrocatalyst reconstruction. *Chem Commun*. 2025;61(4):658–668.
56. Paul S. Hydrogenation and dehydrogenation by catalysis. *Ber Dtsch Chem Ges*. 1911;44:17.
57. Wang K, Xu H, Xing H, Jin L, Qian X, He G, Chen H. Phase-regulated built-in electric field intensity mediates reconstructing for efficient water oxidation. *Chem Eng J*. 2024;500:Article 157316.
58. Zhao S, Shen S-S, Han L, Tian B-C, Li N, Chen W, Li X-B. Ferroelectric perovskite $PbTiO_3$ for advanced photocatalysis. *Rare Metals*. 2024;43(9):4038–4055.
59. Li X, Liu Q, Deng F, Huang J, Han L, He C, Chen Z, Luo Y, Zhu Y. Double-defect-induced polarization enhanced OV-BiOBr/Cu2−xS high-low junction for boosted photoelectrochemical hydrogen evolution. *Appl Catal B Environ*. 2022;314:Article 121502.
60. Mu N, Bo T, Hu Y, Xu R, Liu Y, Zhou W. Single-atom catalysts based on polarization switching of ferroelectric In_2Se_3 for N_2 reduction. *Chin J Catal*. 2024;63:244–257.
61. Li X, Liu H, Chen Z, Wu Q, Yu Z, Yang M, Wang X, Cheng Z, Fu Z, Lu Y. Enhancing oxygen evolution efficiency of multiferroic oxides by spintronic and ferroelectric polarization regulation. *Nat Commun*. 2019;10(1):Article 1409.
62. Li J, Zou Y, Li Z, Fu S, Lu Y, Li S, Zhu X, Zhang T. Modulating the electronic coordination configuration and d-band center in homo-diatomic Fe_2N_6 catalysts for enhanced peroxymonosulfate activation. *ACS Appl Mater Interfaces*. 2022;14(33):37865–37877.
63. Luo D, Yang B, Mei Z, Kang Q, Chen G, Liu X, Zhang N. Tuning the d-band states of Ni-based serpentine materials via Fe^{3+} doping for efficient oxygen evolution reaction. *ACS Appl Mater Interfaces*. 2022;14(47):52857–52867.
64. Li Z, Tian Z, Cheng H, Wang T, Zhang W, Lu Y, Lai Y, He G. Engineering d-band center of FeN4 moieties for efficient oxygen reduction reaction electrocatalysts. *Energy Storage Mater*. 2023;59:Article 102764.
65. Chiang C-H, Lin C-C, Lin Y-C, Huang C-Y, Lin C-H, Chen Y-J, Ko T-R, Wu H-L, Tzeng W-Y, Ho S-Z, et al. Manipulating ferroelectric polarization and spin polarization of 2D $CuInP_2S_6$ crystals for photocatalytic CO_2 reduction. *J Am Chem Soc*. 2024;146(33):23278–23288.
66. Li W, Zhang H, Xu R, Jiang X, Meng H, Xue X-X, Zhang S. Polarization switching-controlled oxygen evolution and reduction reactions for ferroelectric single-atom catalysts. *Chem Eng J*. 2025;505:Article 159247.
67. Lei Y, Ye J, García-Antón J, Liu H. Recent advances in the built-in electric-field-assisted photocatalytic dry reforming of methane. *Chin J Catal*. 2023;53:72–101.
68. Li W, Ma J, Cui G. A multi-physical approach: How ferroelectrics reinforce the performance of secondary batteries. *Nano Energy*. 2024;131:Article 110303.
69. Xu G-R, Wang J, Zhang N, Zhang Q, Dong Z, Zhang W, Wu Z, Xie C-x, Wang L. Ferroelectric polarization promoted electrocatalytic hydrogen evolution on $Bi_2Fe_4O_9$ nanoplates. *Scr Mater*. 2023;232:Article 115509.
70. Lv Z-P, Zhang D-H, Zang M-L, Li S-L, He J-L, Song J-X. Boosting alkaline hydrogen evolution via spontaneous built-in electric field. *Rare Metals*. 2024;43(11):5848–5859.
71. Wu X, Liu X, Deng W, Xiao W, Wang X, Wang G, Wang D, Liu M, Gao C, Wu Y, et al. The synergy of the electric polarization and built-in electric field for efficient OER/ORR supported on 2D ferroelectric TM-gr@Ga_2O_3 heterojunctions

using constant-potential methods. *ACS Sustain Chem Eng*. 2024;12(41):15282–15293.
72. Zhu H, Ren X, Yang X, Liang X, Liu A, Wu G. Fe-based catalysts for nitrogen reduction toward ammonia electrosynthesis under ambient conditions. *SusMat*. 2022;2(3):214–242.
73. Ju L, Ma Y, Tan X, Kou L. Controllable electrocatalytic to photocatalytic conversion in ferroelectric heterostructures. *J Am Chem Soc*. 2023;145(48):26393–26402.
74. Schott CM, Schneider PM, Song K-T, Yu H, Götz R, Haimerl F, Gubanova E, Zhou J, Schmidt TO, Zhang Q, et al. How to assess and predict electrical double layer properties. Implications for Electrocatalysis. *Chem Rev*. 2024;124(22):12391–12462.
75. Luo T, Liu K, Fu J, Chen S, Li H, Pan H, Liu M. Electric double layer structure in electrocatalytic carbon dioxide reduction. *Adv Energy Sustain Res*. 2022;4(3):Article 2200148.
76. Sebastián-Pascual P, Shao-Horn Y, Escudero-Escribano M. Toward understanding the role of the electric double layer structure and electrolyte effects on well-defined interfaces for electrocatalysis. *Curr Opin Electrochem*. 2022;32: Article 100918.
77. Ju L, Tan X, Mao X, Gu Y, Smith S, Du A, Chen Z, Chen C, Kou L. Controllable CO_2 electrocatalytic reduction via ferroelectric switching on single atom anchored In_2Se_3 monolayer. *Nat Commun*. 2021;12(1):Article 5128.
78. Jia P, Li Y, Zheng Z, Wang Y, Liu T. Ferroelectric polarization promotes the excellent CO_2 photoreduction performance of $Bi_4Ti_3O_{12}$ synthesized by molten salt method. *J Alloys Compd*. 2022;920:Article 165880.
79. Tu S, Zhang Y, Reshak AH, Auluck S, Ye L, Han X, Ma T, Huang H. Ferroelectric polarization promoted bulk charge separation for highly efficient CO_2 photoreduction of $SrBi_4Ti_4O_{15}$. *Nano Energy*. 2019;56:840–850.
80. Li S, Bai L, Ji N, Yu S, Lin S, Tian N, Huang H. Ferroelectric polarization and thin-layered structure synergistically promoting CO_2 photoreduction of Bi_2MoO_6. *J Mater Chem A*. 2020;8(18):9268–9277.
81. Ashtar M, Marwat MA, Yang Y, Cao D. Two-dimensional ZnO/ZrXY (X, Y = Br, Cl and F) van der Waals heterostructures as promising photocatalysts for high efficiency water splitting. *Int J Hydrog Energy*. 2023;48(84):32797–32805.
82. Xie J, Yan L, Wang J, Wang G, Sun Z, Zhou L, Yang J, Dong H. Two-dimensional V_2O_3 MOene as promising hydrogen evolution reaction electro-catalyst revealed by first-principles calculations. *Int J Hydrog Energy*. 2024;58: 1587–1595.
83. Yi J, Liao J, Xia K, Song Y, Lian J, She X, Liu Y, Yuan S, Dong F, Xu H, et al. Integrating the merits of two-dimensional structure and heteroatom modification into semiconductor photocatalyst to boost NO removal. *Chem Eng J*. 2019;370:944–951.
84. Tang S, Zhu Y, Li H, Xu H, Yuan S. Two-dimensional carbon nitride-based composites for photocatalytic hydrogen evolution. *Int J Hydrog Energy*. 2019;44(59):30935–30948.
85. Zhang M, Zhou W, Yan X, Huang X, Wu S, Pan J, Shahnavaz Z, Li T, Yu X. Sodium dodecyl sulfate intercalated two-dimensional nickel-cobalt layered double hydroxides to synthesize multifunctional nanomaterials for supercapacitors and electrocatalytic hydrogen evolution. *Fuel*. 2023;333:Article 126323.
86. Ke C, Huang J, Liu S. Two-dimensional ferroelectric metal for electrocatalysis. *Mater Horiz*. 2021;8(12):3387–3393.
87. Cheng M, Si Y, Li N, Guan J. Synergy of charged domain walls in 2D in-plane polarized ferroelectric GeS for photocatalytic water splitting. *J Am Chem Soc*. 2024;146(38):26567–26573.
88. Xiong R, Zhang L, Wen C, Anpo M, Ang YS, Sa B. Ferroelectric switching driven photocatalytic overall water splitting in the as/In_2Se_3 heterostructure. *J Mater Chem A*. 2025; 10.1039/d4ta07884e.
89. Singh D, Joshi B, Poddar P. Ferroelectric polarization and iron substitution synergistically boost electrocatalytic oxygen evolution reaction in bismuth oxychloride nanosheets. *Langmuir*. 2023;39(32):11414–11425.
90. Li S, Zhao Z, Li J, Liu H, Liu M, Zhang Y, Su L, Pérez-Jiménez AI, Guo Y, Yang F, et al. Mechanically induced highly efficient hydrogen evolution from water over piezoelectric SnSe nanosheets. *Small*. 2022;18(29):2202507.
91. Fan Y, Song X, Ai H, Li W, Zhao M. Highly efficient photocatalytic CO_2 reduction in two-dimensional ferroelectric $CuInP_2S_6$ bilayers. *ACS Appl Mater Interfaces*. 2021;13(29):34486–34494.
92. Jiang X, Tan J, Liu D, Feng Y, Chen K-Q, Kazakova EA, Vasenko AS, Chulkov EV. Ferroelectric polarization and single-atom catalyst synergistically promoting CO_2 photoreduction of $CuBiP_2Se_6$. *J Phys Chem Lett*. 2024;15(13):3611–3618.
93. Li M, Young J. Ab initio investigation of tunable CO_2 reduction reaction on the two dimensional ferroelectric Y_2CO_2. *J Mater Chem A*. 2024;12(17):10252–10259.
94. Gunawan M, Zhou S, Gunawan D, Zhang Q, Hart JN, Amal R, Scott J, Valanoor N, Toe CY. Ferroelectric materials as photoelectrocatalysts: Photoelectrode design rationale and strategies. *J Mater Chem A*. 2025.
95. Hu C, Hu Y, Zhang B, Zhang H, Bao X, Zhang J, Yuan P. Advanced catalyst design strategies and in-situ characterization techniques for enhancing electrocatalytic activity and stability of oxygen evolution reaction. *Electrochem Energy Rev*. 2024;7(1):Article 19.
96. Zhao S, Yang Y, Bi F, Chen Y, Wu M, Zhang X, Wang G. Oxygen vacancies in the catalyst: Efficient degradation of gaseous pollutants. *Chem Eng J*. 2023;454:Article 140376.
97. Jiang W, Loh H, Low BQL, Zhu H, Low J, Heng JZX, Tang KY, Li Z, Loh XJ, Ye E, et al. Role of oxygen vacancy in metal oxides for photocatalytic CO_2 reduction. *Appl Catal B Environm*. 2023;321:Article 122079.
98. Guo H, Cui J, Liu L. Research progress in photocatalytic reduction of CO_2 enhanced by oxygen vacancy. *Chin J Appl Chem*. 2020;37(3):256–263.
99. Zhu S, Guo L, Li P, Zhang B, Zhao G, He T. A computational study on linear and bent adsorption of CO_2 on different surfaces for its photoreduction. *Catal Today*. 2019;335: 278–285.
100. Mao J, Mei B, Yang S, Zeng J, Sun F, Chen W, Song F, Jiang Z. In situ oxygen-vacancy engineering for enhancing CO_2 reduction activity. *ACS Mater Lett*. 2024;6(12):5375–5383.
101. Shi J, Chao C, Gao Y, Li H, Ge S, Li C, Chen X, He W. Oxygen vacancies assisted ferroelectric heterojunction for enhanced photocatalytic activity. *Appl Surf Sci*. 2023;624:Article 157144.
102. Yu H, Chen F, Li X, Huang H, Zhang Q, Su S, Wang K, Mao E, Mei B, Mul G, et al. Synergy of ferroelectric polarization and oxygen vacancy to promote CO_2 photoreduction. *Nat Commun*. 2021;12(1):Article 4594.

103. Liu X, Wang J, Zhu F, Li Y, Tian W, Wang W, Guo R, Liu L, Shi J. Surface oxygen vacancy engineering in weak Bi–O bonded ferroelectric bismuth sodium titanate for boosting the photocatalytic CO_2 reduction reaction. *J Mater Chem A*. 2024;12(16):9661–9671.
104. Chen F, Ma Z, Ye L, Ma T, Zhang T, Zhang Y, Huang H. Macroscopic spontaneous polarization and surface oxygen vacancies collaboratively boosting CO_2 photoreduction on $BiOIO_3$ single crystals. *Adv Mater*. 2020;32(11): Article 1908350.
105. Li X, Yu J, Jaroniec M, Chen X. Cocatalysts for selective photoreduction of CO_2 into solar fuels. *Chem Rev*. 2019;119(6):3962–4179.
106. Zhen C, Yu JC, Liu G, Cheng H-M. Selective deposition of redox co-catalyst(s) to improve the photocatalytic activity of single-domain ferroelectric $PbTiO_3$ nanoplates. *Chem Commun*. 2014;50(72):10416–10419.
107. Liu G, Ma L, Yin L-C, Wan G, Zhu H, Zhen C, Yang Y, Liang Y, Tan J, Cheng H-M. Selective chemical epitaxial growth of TiO_2 islands on ferroelectric $PbTiO_3$ crystals to boost photocatalytic activity. *Joule*. 2018;2(6):1095–1107.
108. Yang G, Wang S, Wu Y, Zhou H, Zhao W, Zhong S, Liu L, Bai S. Spatially separated redox cocatalysts on ferroelectric nanoplates for improved piezophotocatalytic CO_2 reduction and H_2O oxidation. *ACS Appl Mater Interfaces*. 2023;15(11):14228–14239.
109. Huang HB, Zhang N, Xu JY, Xu YH, Li YF, Lü J, Cao R. Photocatalytic CO_2–to–ethylene conversion over Bi2S3/CdS heterostructures constructed via facile cation exchange. *Research*. 2022;2022:Article 9805879.
110. Zhang S, Li Y, Gao X, Gao X, Yi Y, Xu D. Bimetallic Ni–Co-ZIF derived (Ni, Co)Se_2/$BiVO_4$ heterojunction photoelectrodes with oxygen vacancy for enhancing PEC performance. *Int J Hydrog Energy*. 2024;55:292–299.
111. Dong H, Hong S, Zhang P, Yu S, Wang Y, Yuan S, Li H, Sun J, Chen G, Li C. Metal-free Z-scheme 2D/2D VdW heterojunction for high-efficiency and durable photocatalytic H_2 production. *Chem Eng J*. 2020;395:Article 125150.
112. Zhu X, Wang Z, Zhong K, Li Q, Ding P, Feng Z, Yang J, Du Y, Song Y, Hua Y, et al. Mo-O-Bi bonds as interfacial electron transport bridges to fuel CO_2 photoreduction via in-situ reconstruction of black Bi_2MoO_6/BiO_{2-x} heterojunction. *Chem Eng J*. 2022;429:Article 132204.
113. Che H, Liu C, Dong H, Li C, Liu X, Che G. Synthesis of mesoporous g-C_3N_4/S-PAN π-conjugation heterojunction via sulfur-induced cyclization reaction for enhanced photocatalytic H2 production. *Int J Hydrog Energy*. 2019;44(36):20029–20041.
114. Huang J, Wang Y, Liu X, Li Y, Hu X, He B, Shu Z, Li Z, Zhao Y. Synergistically enhanced charge separation in $BiFeO_3$/Sn:TiO_2 nanorod photoanode via bulk and surface dual modifications. *Nano Energy*. 2019;59:33–40.
115. Liu L, Zhang Y, Huang H. Junction engineering for photocatalytic and photoelectrocatalytic CO_2 reduction. *Sol RRL*. 2020;5(2):Article 2000430.
116. Low J, Yu J, Jaroniec M, Wageh S, Al-Ghamdi AA. Heterojunction photocatalysts. *Adv Mater*. 2017;29(20):Article 1601694.
117. Wang H, Zhang L, Chen Z, Hu J, Li S, Wang Z, Liu J, Wang X. Semiconductor heterojunction photocatalysts: Design, construction, and photocatalytic performances. *Chem Soc Rev*. 2014;43(15):5234–5244.
118. Shen S, Li X, Zhou Y, Han L, Xie Y, Deng F, Huang J, Chen Z, Feng Z, Xu J, et al. Novel BiOBr/Bi_2S_3 high-low junction prepared by molten salt method for boosting photocatalytic degradation and H_2O_2 production. *J Mater Sci Technol*. 2023;155:148–159.
119. Li X, Wan Y, Deng F, Zhou Y, Chen P, Dong F, Jiang J. Advances in Z-scheme and S-scheme heterojunctions for photocatalytic and photoelectrocatalytic H_2O_2 production. *Chin Chem Lett*. 2025;36(10):Article 111418.
120. Wang X-D, Huang Y-H, Liao J-F, Jiang Y, Zhou L, Zhang X-Y, Chen H-Y, Kuang D-B. In situ construction of a Cs_2SnI_6 perovskite nanocrystal/SnS_2 nanosheet heterojunction with boosted interfacial charge transfer. *J Am Chem Soc*. 2019;141(34):13434–13441.
121. Jia P, Li Y, Zheng Z, Liu Y, Wang Y, Liu T. A dual optimization approach for photoreduction of CO_2 to alcohol in g-C_3N_4/$BaTiO_3$ system: Heterojunction construction and ferroelectric polarization. *Appl Surf Sci*. 2022;602:Article 154310.
122. Pan D, Lu Y, Idris AM, Chen Z, Xu L, Wang J, Jiang G, Chen Z, Li Z. Enhancing photocatalytic CO_2 reduction via a single-domain ferroelectric Z-scheme heterojunction of $BiFeO_3$/$CsPbBr_3$ inducing dual built-in electric fields. *J Mater Chem A*. 2024;12(17):10461–10471.
123. Fu J, Xu Q, Low J, Jiang C, Yu J. Ultrathin 2D/2D WO_3/g-C_3N_4 step-scheme H2-production photocatalyst. *Appl Catal B Environ*. 2019;243:556–565.
124. Guo H, Jiang J, Liang J, Wen C, Xi X, Dong P. Achieving remarkable charge transfer through the depolarization field in the 2D/2D S-scheme heterojunction consisted of C_3N_5 nanosheets and layered ferroelectric Bi_3TiNbO_9 for photocatalytic hydrogen production. *Chem Eng J*. 2025;504:Article 158649.
125. Alawode BO, Kolpak AM. $PbTiO_3$(001) capped with ZnO($11\bar{2}0$): An ab initio study of effect of substrate polarization on interface composition and CO_2 dissociation. *J Phys Chem Lett*. 2016;7(7):1310–1314.
126. Qiao B, Wang A, Yang X, Allard LF, Jiang Z, Cui Y, Liu J, Li J, Zhang T. Single-atom catalysis of CO oxidation using Pt_1/FeO_x. *Nat Chem*. 2011;3(8):634–641.
127. Gao S, Yang H, Rao D, Wang N, Li Y, Li J, Rao S, Maouche C, Wu Z, Li B, et al. Supercritical CO_2 assisted synthesis of highly accessible iron single atoms and clusters on nitrogen-doped carbon as efficient oxygen reduction electrocatalysts. *Chem Eng J*. 2022;433:Article 134460.
128. Liu X, He F, Lu Y, Wang S, Zhao C, Wang S, Duan X, Zhang H, Zhao X, Sun H, et al. The double-edged effect of single atom metals on photocatalysis. *Chem Eng J*. 2023;453:Article 139833.
129. Xie S, Zhang Q, Liu G, Wang Y. Photocatalytic and photoelectrocatalytic reduction of CO_2 using heterogeneous catalysts with controlled nanostructures. *Chem Commun*. 2016;52(1):35–59.
130. Inoue T, Fujishima A, Konishi S, Honda K. Photoelectrocatalytic reduction of carbon dioxide in aqueous suspensions of semiconductor powders. *Nature*. 1979;277(5698):637–638.
131. Ma H, Ye X, Li X, Xu ZJ, Sun Y. Ferroelectric polarization effects of single-atom catalysts on water oxidation. *Adv Mater*. 37(21):Article e2500285.
132. Liu L, Hu J, Ma Z, Zhu Z, He B, Chen F, Lu Y, Xu R, Zhang Y, Ma T, et al. One-dimensional single atom arrays on

ferroelectric nanosheets for enhanced CO_2 photoreduction. *Nat Commun*. 2024;15(1):Article 305.
133. Cao C, Zhou S, Zuo S, Zhang H, Chen B, Huang J, Wu X-T, Xu Q, Zhu Q-L. Si doping-induced electronic structure regulation of single-atom Fe sites for boosted CO_2 electroreduction at low overpotentials. *Research*. 2023;6:Article 0079.
134. Yang Y, Liu S, Fu G. Electrochemical reduction of CO_2 via single-atom catalysts supported on α-In_2Se_3. *J Phys Chem Lett*. 2023;14(26):6110–6118.
135. Yang H, Zou W, Zhang C, Du A. Ab initio studies of electrocatalytic CO_2 reduction for small Cu cluster supported on polar substrates. *ACS Appl Mater Interfaces*. 2024;16(26):33688–33695.
136. Zhang X, Wan Y, Wen Y, Zhu Y, Liu H, Qiu J, Zhu Z, Sun Z, Gao X, Bai S, et al. SnSe nanosheets with Sn vacancies catalyse H_2O_2 production from water and oxygen at ambient conditions. *Nat Catal*. 2025;8(5):465–475.
137. Liu H, Li S, Liu M, Sun P, Zhang X, Zhang L, Zhang Y, Contreras-Jiménez G, Potier J, Sun Z, et al. Mechanically driven selective organic oxidation using MOF-coated piezoelectric SnSe nanosheets. *Nano Energy*. 2025;142:Article 111241.
138. Li S, Liu X, Zhang X, Liu Y. Bi_2O_2Se nanosheets for efficient piezocatalytic H_2O_2 production. *Catalysts*. 2025;15(2):157.
139. Li H, Sang Y, Chang S, Huang X, Zhang Y, Yang R, Jiang H, Liu H, Wang ZL. Enhanced ferroelectric-nanocrystal-based hybrid photocatalysis by ultrasonic-wave-generated piezophototronic effect. *Nano Lett*. 2015;15(4):2372–2379.
140. Pan H, Lan S, Xu S, Zhang Q, Yao H, Liu Y, Meng F, Guo E-J, Gu L, Yi D. Ultrahigh energy storage in superparaelectric relaxor ferroelectrics. *Science*. 2021;374(6563):100–104.
141. Liu X, Wang Y, Tian W, Zhu F, Wang J, Wang W, Li Y, Zeng K, Shi J. Strong interfacial interaction in polarized ferroelectric heterostructured nanosheets for highly efficient and selective photocatalytic CO_2 reduction. *Small*. 2025;21(8):Article 2409801.